Recent progress of nuclear liquid gas phase transition

MA Yu-Gang, SHEN Wen-Qing

(Shanghai Institute of Applied Physics, the Chinese Academy of Sciences, Shanghai 201800)

Abstract Recent progress on nuclear liquid gas phase transition (LGPT) has been reviewed, especially for the signals of LGPT in heavy ion collisions. These signals include the power-law charge distribution, cluster emission rate, nuclear Zipf law, bimodality, the largest fluctuation of the fragments, Δ-scaling, caloric curve, phase coexistence diagram, critical temperature, critical exponent analysis, negative specific heat capacity and spinodal instability etc. The systematic works of the authors on experimental and theoretical LGPT are also introduced.

Keywords Nuclear liquid gas phase transition, Fragment yield distribution, Fisher droplet model, Zipf-type law, Fluctuation observables, Caloric curve, Phase coexistence diagram, Critical exponent, Spinodal instability

CLC numbers O414.13, O571.6

1 Introduction

Phase transition and critical phenomenon is an extensively debatable subject in the natural sciences. Recently, the same concept was introduced into the astronomical objects[1] and the microscopic systems, such as in atomic cluster[2] and nuclei,[3] of which the nuclei, as a microscopic finite-size system, are attracting more and more nuclear experimentalists to search for the liquid−gas phase transition (LGPT) and investigate its behavior. To date, various experimental evidences have cumulated which seem to be related to the nuclear phase transition. For instance, violent heavy-ion collisions break the nuclei into several intermediate mass fragments (IMF), which can be viewed as a critical phenomenon as observed in fluid, atomic and other systems. It prompts a possible signature on the liquid−gas phase transition in the nuclear system. The sudden opening of the nuclear multifragmentation and vaporization[4] channels can be interpreted as the signature of the boundaries of phase mixture. In addition, the plateau of the nuclear caloric curve[5] in a certain excitation energy range gives a possible indication of a first-order phase transition[6,7] as predicted in the framework of statistical equilibrium models.[8] On the other hand, the extraction of critical exponents in the charge or mass distribution of the multifragmentation system[9] can be explained as an evidence of phase transition. More recently, the negative microcanonical heat capacity was experimentally observed in nuclear fragmentation[10] which relates to the liquid−gas phase transition,[11] and in atomic cluster[12] which relates to solid to liquid phase transition,[13] respectively. Moreover, some evidence of spinodal decomposition in nuclear multifragmentation was recently obtained experimentally,[14] which shows the presence of liquid-gas phase coexistence region and gives a strong argument in favor of the existence of first-order liquid-gas phase transition in finite nuclear systems. Δ-scaling of the largest fragment was also investigated recently and it shows to be a good probe to detect the phase change.[15] The nuclear Zipf's law and multiplicity information entropy (H) were defined and proposed to diagnose the onset of liquid-gas phase transition.[16,17] Phase coexistence diagram was also constructed based on EOS data.[18,19]

Meanwhile, several theoretical models have been developed to treat such a phase transition in the nuclear disassembly, e.g. percolation model, lattice gas model, statistical multifragmentation model and molecular dynamics model etc (e.g. see the recent review articles[20-22] and references therein). In this article, we

Supported by the National Natural Science Foundation of China for the Distinguished Young Scholar (No. 19725521), the National Natural Science Foundation of China (No. 19705012), the Science and Technology Development Foundation of Shanghai (No. 97QA14038) and the Major State Basic Research Development Program of China (No. G200077400)

Received date: 2003-12-24

will introduce the recent progress on nuclear LGPT in experimental observation and theoretical treatment.

The paper is organized as follows. Section 2 introduces the selected models for investigating the nuclear liquid gas phase transition, which include the mean field theory, percolation model, statistical multifragmentation model, lattice gas model (LGM) and classical molecular dynamics (CMD) model etc. Section 3 presents the extensive signatures for LGPT. Finally a simple summary is given in Section 4.

2 Selected models for nuclear LGPT

2.1 Nuclear mean field theory

Nuclear matter is an idealized system of equal number of neutrons N and protons Z. The system is very large and the Coulomb interaction between protons is switched off. Due to the existence of Coulomb interaction, stable systems are scarce after mass number $A = N+Z > 260$, so no known nuclei approach the limit of nuclear matter. However, the extrapolation from known nuclei causes one to deduce that nuclear matter has density $\rho_0 \approx 0.16 \text{fm}^{-3}$ and binding energy ≈ 16 MeV/A. Usually the Equation of State (EOS) of the idealized nuclear matter is used to examine if a liquid-gas phase transition can be expected and at what temperature and density.

The Skyrme parametrization for the interaction potential energy has been demonstrated[23,24] to be a good approximation for Hartree-Fock calculations. A set of isotherms for an equation of state (pressure versus density) corresponding to nuclear forces (Skyrme effective interaction) is shown in Fig.1. In this figure isotherms are drawn for various temperatures (10, 12, 14, 15, 15.64 and 17 MeV). The pressure contributed by kinetic energy was calculated in the finite temperature Fermi-gas model. The similarity with Van der Waals EOS is obvious. With the parameters chosen here the critical temperature is 15.64 MeV. The spinodal region ($\partial p / \partial \rho < 0$) can be seen clearly. The coexistence curve which is shown in the figure is obtained using a Maxwell construction.[25]

Even though mean-field theory, as described above, predicts a liquid-gas phase transition picture, many improvements have to be made if considering the real heavy ion collision case. If Coulomb interaction and finite size effect are taken into account, the "boiling" temperature (i.e. 15.64 MeV from Fig.1) will come down.[26,27] For instance, in mean-field Thomas-Fermi theory that includes the Coulomb interaction[28] a peak in specific heat at 10 MeV for ^{150}Sm was found. Without the Coulomb interaction, in bulk matter with the same isospin asymmetry as ^{150}Sm, the peak is located at 13 MeV. As will be described later, both experimental data and more realistic models point to much lower temperature when phase change occurs.

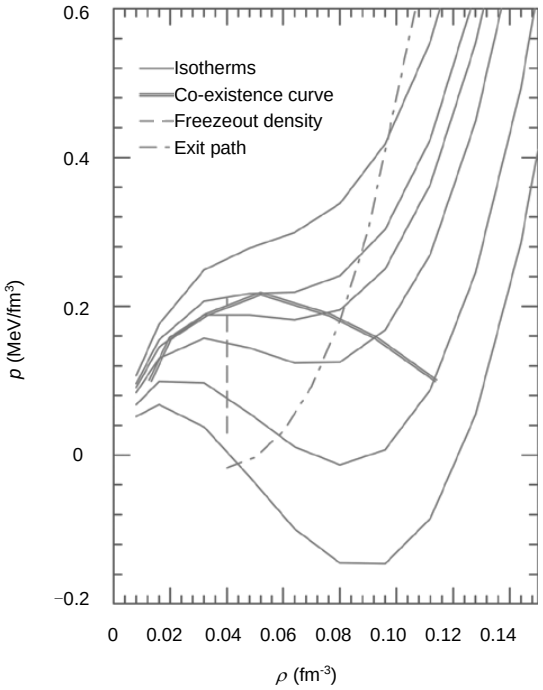

Fig.1 Nuclear matter equation of state with Skyrme interaction with compressibility 201 MeV. In ascending order the isothermals are at temperatures 10, 12, 14, 15, 15.64 (critical isotherm) and 17 MeV. The coexistence curve obtained from a Maxwell construction is shown. The vertical line is drawn at assumed freeze-out density 0.04 fm^{-3}. The dot-dash line is obtained by assuming that the excited system expands isentropically (see Fig.2). This is an idealization from Ref. [21].

2.2 The percolation model

The percolation has been extensively studied in condensed matter physics.[29] The applications in nuclear physics were made by Bauer *et al*[30,31] and Campi *et al*.[32,33]

There are two types of percolation models: site percolation and bond percolation. For applications to nuclear physics, bond percolation was used. In bond percolation there are N lattice sites. One uses a three-dimensional cubic lattice. The number of nucle-

ons is also N. Each lattice site contains one nucleon which is not distinguished between neutrons and protons. The crucial parameter is the bonding probability p whose value can vary between 0 and 1. The probability that two nearest neighboring nucleons will be part of a cluster is given by the value of p. If p=0 (e.g. in the case of high excitation energy) all N^3 nucleons will emerge as singles. If p=1, the nucleons stay together as one nucleus (e.g. in the case of low excitation energy, not enough to break up the nucleus). For the values of p between the two extremes Monte-Carlo sampling is needed to generate events and determine in each event the occurrence of clusters of different sizes. There is a phase transition in this model. One can define a percolating cluster; this is a cluster, which, if it exists, spans the walls, i.e. connects opposite walls through an unbroken cluster. For N very large, this appears at the value of p=0.2488. This value of p will be labelled by p_c. The order parameter in this model is the probability that an arbitrary site (equivalently an arbitrary nucleon) is part of this percolating cluster. Below p_c, this is zero since there is no percolating cluster. It starts from zero at p_c and continuously moves towards the value 1 as the value of p is increased. The phase transition in this model is continuous and not a first-order phase transition. Near critical points, one can define critical exponents and try to evaluate them from experiment. We will see later that even though we now regard the phase transition in nuclear heavy ion collisions to be first order, it is meaningful to try to measure certain critical exponents.

2.3 Statistical multifragmentation model

Statistical multifragmentation models have been very successful in explaining processes in heavy-ion collisions. These models define a freeze-out volume. At this volume an equilibrium statistical mechanics calculation is done. However, these statistical calculations do not start from a fundamental two-body interaction or even a simplified schematic two-body interaction. Instead, the inputs are the properties of the composites (which appear as bound objects because of the fundamental two-body interaction); their binding energies and the excited states. Their populations are solely dictated by phase-space. This is very similar to chemical equilibrium between perfect gases as, for example, discussed in [25]. The only interaction between composites is that they can not overlap with each other in the configuration space. Coulomb interaction between composites can be taken into account in different stages of approximation. These models have the virtue that they can be used to calculate data for many experiments whether these experiments relate to phase transition or not. The Copenhagen model, a statistical multifragmentation model abbreviated SMM, has become the "shell-model" code for intermediate energy heavy ion data. An excellent review of this model exists.[34] The Berlin Model, a microcanonical multifragmentation model, usually abbreviated MMMC, has also been used to fit experimental data.[35] Some other references for microcanonical simulation of similar physics are [36]~[38]. While there have been tremendous improvements in techniques and details, the roots of such models for heavy-ion collisions go back 1970s.[39]

With some simplifications, the model of composites within the freeze-out volume at a given temperature can be exactly solved, as phase transition aspects are easily studied in the model. It should be mentioned that a peak in the specific heat at about 5 MeV temperature was predicted in the model well before experiments were done.[40]

2.4 Lattice gas model and molecular dynamics model

The lattice gas model of Lee and Yang,[41] where the grand canonical partition function of a gas with one type of atoms is mapped into the canonical ensemble of an Ising model for spin 1/2 particles, has successfully described the liquid-gas phase transition for the atomic system. The same model has already been applied to the microscopic nuclear system, e.g. see the papers [42]~[48].

In the LGM, A (= N + Z) nucleons with an occupation number s, which is defined as the 'spin' s=1(-1) for a proton (neutron) or s=0 for a vacancy, are placed in the L sites of a three-dimensional cubic lattice. Each cubic lattice has a size $1.0/\rho_0$= 6.25 fm^3 and can, at most, be occupied by a single nucleon, where ρ_0=0.16 fm^{-3} is the normal nucleon density. Nucleons in the nearest neighboring sites interact with an energy

$\varepsilon_{s_i s_j} s_i s_j$. The Hamiltonian of the system is written as

$$H = \sum_{i=1}^{A} \frac{P_i^2}{2m} - \sum_{i<j} \varepsilon_{s_i s_j} s_i s_j \tag{1}$$

The interaction constant $\varepsilon_{s_i s_j}$ is related to the binding energy of the nuclei. In order to incorporate the isospin effect in the LGM (thereafter, we will called "I-LGM"), the short-range interaction constant $\varepsilon_{s_i s_j}$ is chosen to be different between the nearest neighboring like nucleons and unlike nucleons,

$$\begin{aligned} \varepsilon_{\mathrm{nn}} &= \varepsilon_{\mathrm{pp}} = 0\,\mathrm{MeV} \\ \varepsilon_{\mathrm{pn}} &= -5.33\,\mathrm{MeV} \end{aligned} \tag{2}$$

which indicates the repulsion between the nearest-neighboring like nucleons and attraction between the nearest-neighboring unlike nucleons. This kind of isospin-dependent interaction incorporates, to a certain extent, the Pauli exclusion principle and effectively avoids producing unreasonable clusters, such as di-proton and di-neutron clusters etc. The disassembly of the system is calculated at an assumed 'freeze-out' density $\rho_f = (A/L)\,\rho_0$, beyond ρ_f nucleons are too far apart to interact.

In this model, (N+Z) nucleons are put in L sites by Monte Carlo sampling using the canonical Metropolis algorithm.[49] Various observables based on phase space can be calculated in a straightforward fashion for each event. The cluster distribution in LGM can be obtained by using the rule that two nucleons are part of the same cluster if their relative kinetic energy is insufficient to overcome the attractive bond:[44]

$$(P_r^2 / 2\mu) - \varepsilon_{s_i s_j} s_i s_j < 0 \tag{3}$$

This method has been proved to be similar to the so-called Coniglio-Klein prescription in condensed matter physics[50] and was shown to be valid in LGM.

Since LGM is a model of the nearest-neighboring interaction, a long-range Coulomb force is not amenable to lattice gas type calculation. Pan and Das Gupta[41,43] provide a prescription, based on simple physical reasoning, to decide if two nucleons, occupying neighboring sites form part of the same cluster or not.[51] They first tried to map the LGM calculation to a classical molecular dynamics type prediction, both first carried out without any Coulomb interaction. If the calculations match quite faithfully, then they can study the effects of the Coulomb interaction by adding that to the molecular dynamics calculation. The starting point of CMD is a thermally equilibrated source which has been produced by the above I-LGM: i.e. the nucleons are initialized at their lattice sites with Metropolis sampling and have their initial momenta with Maxwell-Boltzmann sampling. From this starting point we switch the calculation to CMD evolution under the influence of a chosen force. Note that in this case ρ_f is, strictly speaking, not a 'freeze-out' density for molecular dynamics calculation but merely defines the starting point for time evolution. However, since classical evolution of a many particle system is entirely deterministic and the initialization does have in it all the information of the asymptotic cluster distribution, we continue to call ρ_f the 'freeze-out' density.

The form of the force in the CMD is also chosen to be isospin dependent in order to compare with the results of I-LGM. The potential for unlike nucleons is expressed as[43,52]

$$\begin{aligned} &\upsilon_{\mathrm{np}}(r) = C[B(r_0/r)^p - (r_0/r)^q]\exp[\frac{1}{(r/r_0)-a}], \quad (r/r_0 < a) \\ &\upsilon_{\mathrm{np}}(r) = 0, \qquad (r/r_0 > a) \end{aligned} \tag{4}$$

where r_0=1.842 fm is the distance between the centers of two adjacent cubes so that $\rho_0 = 1/r_0^3 = 0.16$ fm^{-3}. The parameters of the potentials are p = 2, q = 1, a = 1.3, B =0.924 and C = 1966 MeV. With these parameters the potential is minimum at r_0 with the value -5.33 MeV and zero when the nucleons are more than 1.3 r_0 apart and strongly repulsive when r is significantly less than ρ_0. We now turn to the nuclear potential between like nucleons. Although we take $\varepsilon_{\mathrm{pp}} = \varepsilon_{\mathrm{nn}} = 0$ in I-LGM, the fact that we do not put two like nucleons in the same cube suggests that there is short-range repulsion between them. We have taken the nuclear force between two like nucleons to be the same expressions as above +5.33 MeV up to r = 1.842 fm and zero afterwards,

$$\begin{aligned} &\upsilon_{\mathrm{pp}}(r) = \upsilon_{\mathrm{np}}(r) - \upsilon_{\mathrm{np}}(r_0), \qquad (r < r_0) \\ &\upsilon_{\mathrm{pp}}(r) = 0, \qquad (r > r_0) \end{aligned} \tag{5}$$

Fig.2 shows the above potential υ_{np} or υ_{pp}.[53] This potential form automatically cuts off at $r/r_0 = a$ (Eq.4) or r/r_0=1 (Eq.5) without discontinuities in any r derivatives, which is a distinct advantage in any molecular dynamics simulation application.

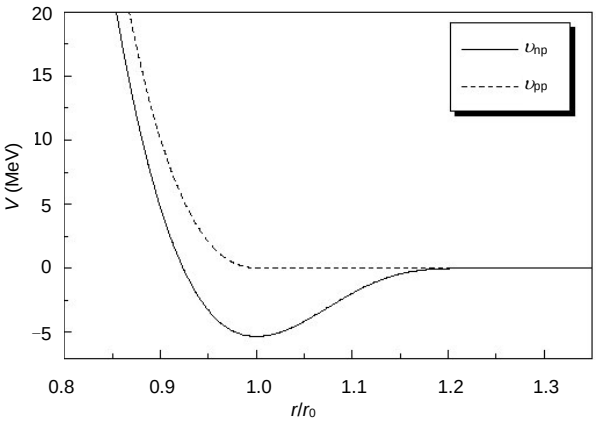

Fig.2 Molecular dynamics potential for like nucleon pair (υ_{pp}) and unlike nucleon pair (υ_{np}). From Ref. [53].

The system evolves with the above potential. The time evolution equations for each nucleon are, as usual, given by

$$\partial \overrightarrow{p_i} / \partial t = -\sum\nolimits_{j \neq i} \nabla_i \upsilon(r_{ij}),$$
$$\partial \vec{r}_i / \partial t = \overrightarrow{p_i} / m. \quad (6)$$

Numerically, the particles are propagated in the phase space by a well-known Verlet algorithm,[54] one of the finite-difference methods in molecular dynamics with continuous potentials. At asymptotic times, for instance, the original blob of matter expands to 64 times its volume in the initialization, the clusters are easily recognized: nucleons which stay together after an arbitrarily long time are part of the same cluster. The observables based on cluster distribution in both models are now compared while they are also compared by switching on/off the Coulomb interaction within the molecular dynamics.

3 Signatures of the nuclear liquid gas phase transition

3.1 Fisher droplet model: power law of charge/mass distribution

The Fisher droplet model has been extensively applied to the analysis of multifragmentation since the pioneering experiments on high energy proton-nucleus collisions by the Purdue group.[3,55,56] Relative yields of fragments with $3 \leqslant Z \leqslant 14$ could be well described by a power law dependence $A^{-\tau}$ and suggested that this might reflect the disassembly of a system whose excitation energy was comparable to its total binding energy.[55] The extracted value of power-law exponent was $2 \leqslant \tau \leqslant 3$, which is in a reasonable range for critical behavior.[57] This success of this approach suggested that the multi-fragmentation of nuclei might be analogous to a continuous liquid to gas phase transition observed in more common fluids.

In the Fisher droplet model the fragment mass distribution may be represented as

$$Y(A) = Y_0 A^{-\tau} X^{A^{2/3}} Y^A \quad (7)$$

where Y_0, τ, X and Y are parameters. However, at the critical point X=1 and Y=1 and the cluster distribution is given by a pure power law

$$Y(A) = Y_0 A^{-\tau} \quad (8)$$

The model predicts a critical exponent τ~2.21.

In this paper, we will use some results which were recently obtained in Cyclotron Institute, Texas A&M University to show some signatures of nuclear LGPT.[58] Of course, many other works are also included in this review article. For the former work, we used Ar + Ni reaction at 47 MeV/nucleon and reconstructed the quasi-projectile (QP) using a new method which is based on three source fits and the Monte Carlo sampling for the assignment of QP.[59] Well defined QP sources have been obtained and their disassembly features have been analyzed. For simplicity, we call experimental data of this work as TAMU data.[58]

Firstly, in Fig.3 we present, for the QP from the reactions of ^{40}Ar+^{58}Ni, yield distributions, dN/dZ, observed for nine different excitation energy (E*/A) intervals from TAMU data.

At low excitation energy a large Z residue always remains, i.e. the nucleus is basically in the liquid phase accompanied by some evaporated light particles. When E*/A reaches ~6.0 MeV/nucleon, this residue is much less prominent. As E*/A continues to increase, the charge distributions become steeper, which indicates that the system tends to vaporize. To quantitatively pin down the possible phase transition point, we use a power law fit to the QP charge distribution in the range of Z=2~7 to extract the effective Fisher-law parameter τ_{eff} by

$$\mathrm{d}N / \mathrm{d}Z \sim Z^{-\tau_{\text{eff}}} \quad (9)$$

The open squares of Fig.4 show τ_{eff} vs excitation energy, a minimum with τ_{eff}~2.3 is seen to occur in the

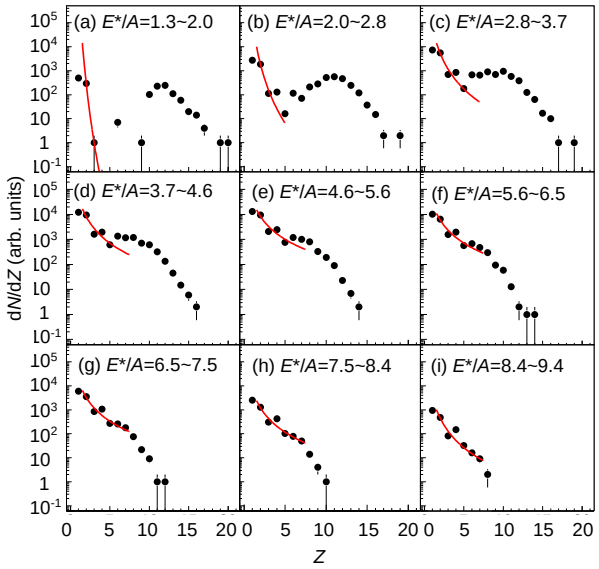

Fig.3 Charge distribution of QP in different E^*/A (in unit of MeV/nucleon) window. From TAMU data.[58]

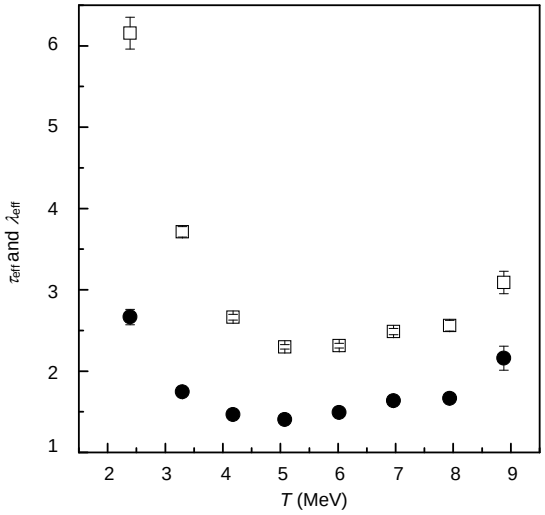

Fig.4 $\tau_{\rm eff}$ (open squares) and $\lambda_{\rm eff}$ (solid circles) as a function of excitation energy. From TAMU data.[58]

E^*/A range of 5 to 6 MeV/nucleon. $\tau_{\rm eff}$~2.3 is close to the critical exponent of the liquid gas phase transition universality class as predicted by Fisher's droplet model.[57] The observed minimum is rather broad.

In a lattice gas model investigation of scaling and apparent critical behavior, Gulminelli *et al*. have pointed out that, in finite systems, the distribution of the maximum size cluster, i.e. the liquid, might overlap with the gas cluster distribution in such a manner as to mimic the critical power law behavior with $\tau_{\rm eff}$~2.2.[60] They further note, however, that at that point the scaling laws are satisfied, which indicates a potentially more fundamental reason for the observation of the power law distribution.[60] Assuming that

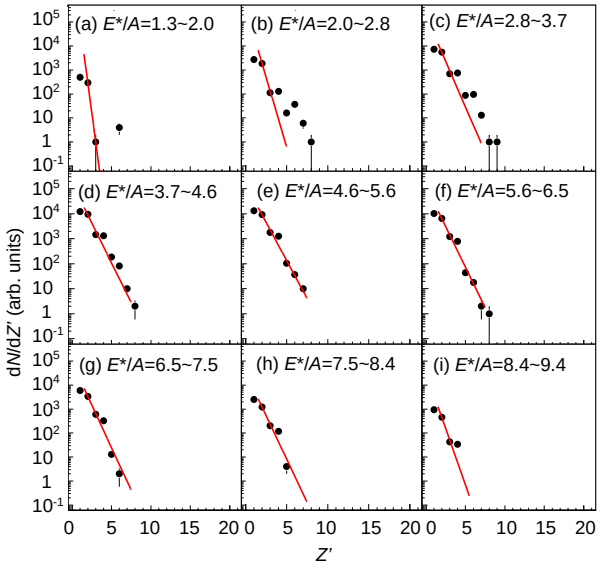

Fig.5 The same as Fig.3 but the heaviest cluster is excluded on the event-by-event basis. From TAMU data.[58]

the heaviest cluster in each event represents the liquid phase, we have attempted to isolate the gas phase by event-by-event removal of the heaviest cluster from the charge distributions. We find that the resultant distributions are better described as exponential as seen in Fig.5.

The fitting parameter $\lambda_{\rm eff}$ of this exponential form $\exp(-\lambda_{\rm eff} Z')$ was derived and is plotted against excitation energy in Fig.4. A minimum is seen in the same region where $\tau_{\rm eff}$ shows a minimum. The minima of $\tau_{\rm eff}$ and $\lambda_{\rm eff}$ indicate the onset of phase change.

3.2 Cluster emission rate

In heavy ion collisions, the emission of particles is an important observable. In the framework of the isospin dependent lattice gas model (I-LGM) and classical molecular dynamics (I-CMD), we studied the relationship of particle emission and liquid gas phase transition. Fig.6 shows that the mean multiplicities between emitted neutrons, protons, charged particles (CP) and intermediate mass fragments (IMF, i.e. $3 \leqslant Z \leqslant 20$) and the mean mass for the largest fragment evolve with temperature at different 'freeze-out' densities ρ_f=0.097ρ_0, 0.18ρ_0, 0.38ρ_0 and 0.60ρ_0 for ^{129}Xe, in the I-CMD calculation.[53] At a fixed 'freeze-out' density, average neutron multiplicity ($N_{\rm n}$), proton multiplicity ($N_{\rm p}$), charged particle multiplicity ($N_{\rm cp}$) and the mean mass for the largest fragment ($A_{\rm max}$) display monotonous increase or decrease with temperature as

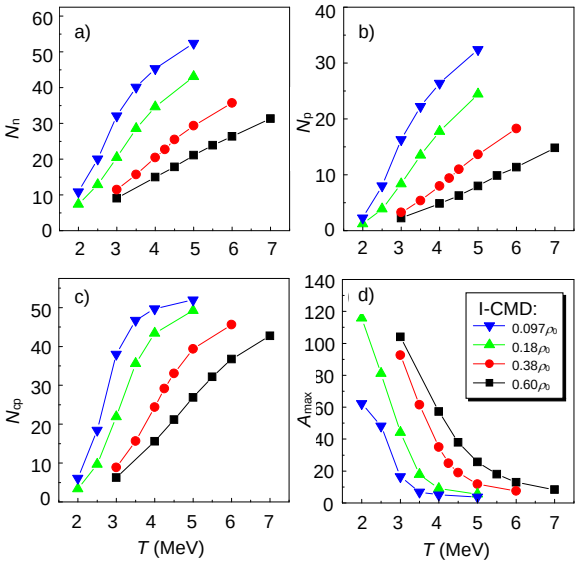

Fig.6 Average multiplicity of the emitted neutrons N_n (a), protons N_p (b), charged particles N_{cp} (c) and the mean mass of the largest fragment A_{max} (d) as a function of temperature in different 'freeze-out' density in the framework of I-CMD. The symbols are illustrated in the right bottom corner. From Ref.[53].

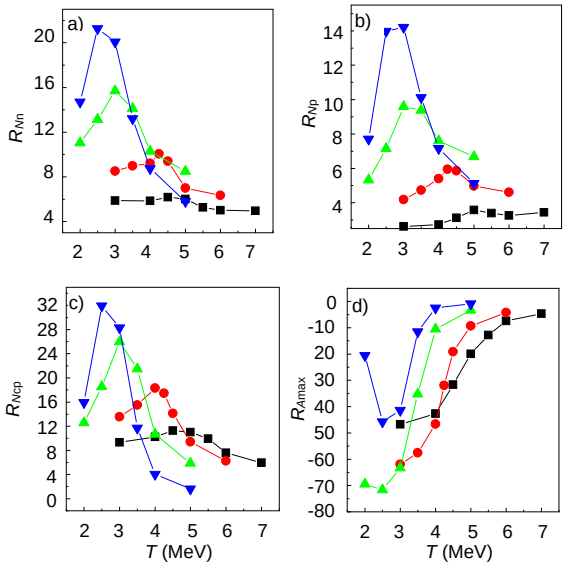

Fig.7 The same as in Fig.6, but for their slopes with temperature. The symbols are the same as in Fig.6. From Ref.[53].

expected. With decreasing 'freeze-out' density, N_p, N_n and N_{cp} increase, since larger space separation among nucleons at smaller 'freeze-out' density makes the clusters less bound and therefore the sizes of free clusters decrease and then the cluster multiplicities increase.

It seems difficult to discover the possibility of phase transition of nuclei if we only see these mean quantities as shown above. However, when we focus on their slopes to temperature (Fig.7), sharp changes are observed at nearly the same temperature at each fixed 'freeze-out' density, for instance, namely around 3, 3.5, 4.5, 5 MeV at ρ_f=0.097ρ_0, 0.18ρ_0, 0.38ρ_0 and 0.60ρ_0, respectively. At such a transition point, (1) the multiplicities of emitted clusters increase rapidly and after that the emission rate slows down; and (2) the decrease in the largest fragment size reaches a valley for such a finite system. Physically, the largest fragment is simply related to the order parameter $\rho_l - \rho_g$ (the difference of density in nuclear 'liquid' and 'gas' phases). In infinite matter, the infinite cluster exists only on the 'liquid' side of the critical point. In finite matter, the largest cluster is present on both sides of the phase transition point. In this calculation, a valley for the slope of A_{max} to temperature may correspond to a sudden disappearance of infinite cluster ('bulk liquid') near the phase transition temperature. It is not the occasional production of such waves of the slopes; it should reflect the onset of phase transition there. This idea is supported by surveying the other phase transition observables, such as the effective power law parameter τ_{eff} from the mass or charge distribution of fragment and the information entropy H of event multiplicity distribution.[16]

3.3 Rise and fall of multi-fragment emission

Copious emission of intermediate mass fragments is one predicted consequence of the liquid-gas phase transition of nuclear matter, by both statistical models and transport models. At low excitation energy, few fragments are "evaporated" from the liquid while at very high excitation energy, the liquid "vaporizes" to produce a nucleon gas. The "rise and fall" of IMF multiplicities has been observed in both central and peripheral collisions. For instance, for central collisions, maximum fragment productions occur around incident energy of 100A MeV for the Kr+Au reaction.[61-63] Fragment multiplicities increase to a maximum with increasing excitation energy. The fragment production then declines and "vaporizes" completely into nucleons and light particles.

Similar to the particle emission, we investigated the IMF emission. Here IMF is defined as $3 \leqslant Z \leqslant 20$. Fig.8 shows the mean multiplicity of IMF of ^{129}Xe as a function of temperature in different freeze-out densities in I-CMD calculation. The multiplicity (N_{imf}) of IMF shows a rise and fall with temperature,[53] when

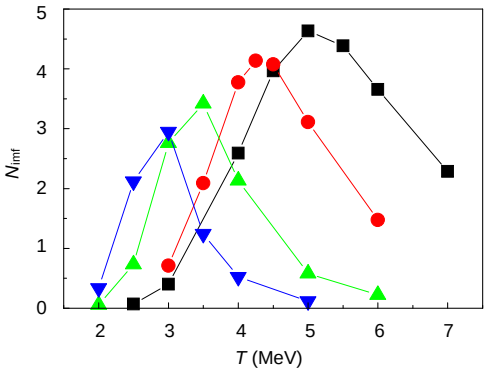

Fig.8 Average multiplicity of IMF as a function of temperature in different 'freeze-out' density in the framework of I-CMD. The symbols are the same as in Fig.6. From Ref.[53].

the system probably crosses the phase transition boundary. The peak position of N_{imf} is close to the turning point of the emission rate as Fig.7 shows. This kind of onset of the multifragments reflects the phase change of nuclei.

In our earlier work with the quantum molecular dynamics model,[64] we also investigated the IMF production as a function of beam energy. The similar rise and fall has been observed. For Ar+Al system in central collisions, a peak of IMF production is observed around 65 MeV/nucleon. Combined with other observables, such as effective τ and λ parameters of charge distributions, the fluctuation analysis (Campi plots, see below) illustrates that the rise and fall of IMF production correspond to liquid gas phase transition.[64]

3.4 Fragment hierarchical distribution: Zipf plot and Zipf law

In addition to the fragment emission and its spectra, observables revealing some particular topological structure may also reflect the critical behavior for a finite system. In this section we discuss two observables: nuclear Zipf law and the correlation between the largest two fragments.

Recently, Ma proposed measurements of the fragment hierarchy distribution as a tool to search for the liquid gas phase transition in a finite nuclear system with help of lattice gas model and classical molecular dynamics model.[16,65] The fragment hierarchy distribution can be defined by the so-called Zipf plot, i.e. a plot of the relationship between mean sizes of fragments which are rank-ordered in size, i.e. largest, second largest, etc. and their rank.[16] Originally the Zipf plot was used to analyze the hierarchy of usage of words in a language,[66] i.e. the relative population of words ranging from the word used most frequently to the word used least frequently. The integer rank was defined starting from 1 for the most probable word and continuing to the least probable word. Surprisingly, a linear relationship between the frequency and the order of words was found. Later, many applications of this relationship were made in a broad variety of areas, such as population distributions, sand-pile avalanches, the size distribution of cities, the distribution in strengths of earthquakes, the genetic sequence and the market distribution of sizes of firms, etc. It has been suggested that the existence of very similar linear hierarchy distributions in these very different fields indicates that Zipf's law is a reflection of self-organized criticality.[67]

In such an analysis, the cluster size is employed as the variable to make a Zipf-type plot, and the resultant distributions are fitted with a power law,

$$< Z_{\rm rank} > \propto {\rm rank}^{-\lambda} \tag{10}$$

where λ is the Zipf's law parameter. Fig.9 shows the Zipf-type plots for the disassembly of Xe with I-LGM calculations. The fit parameter λ was extracted in each temperature. When λ~1, Zipf's law is satisfied. In this case, the mean size of the second largest fragment is 1/2 of that of the largest fragment. That of the third largest fragment is 1/3 of the largest fragment, etc. The upper panels of Fig.10 shows the fitted λ parameters as a function of temperature. The lower panels show their χ^2/ndf, the minimum indicates the best fit for power law when Zipf law is satisfied. To further approve the relationship of Zipf law with the liquid gas phase transition, we show the results of some other physical observables, namely the effective power-law parameter, τ, the second moment of the cluster distribution, S_2, and the multiplicity of intermediate mass fragments, N_{imf}, for the disassembly of ^{129}Xe: Fig.11. These observables were shown to be good indicators of a liquid gas phase transition, as shown in the above sections and Ref. [68]. The extreme values of τ, N_{imf} and S_2 occur at the same temperature, indicating the onset of the phase transition, which is consistent with the temperature where Zipf

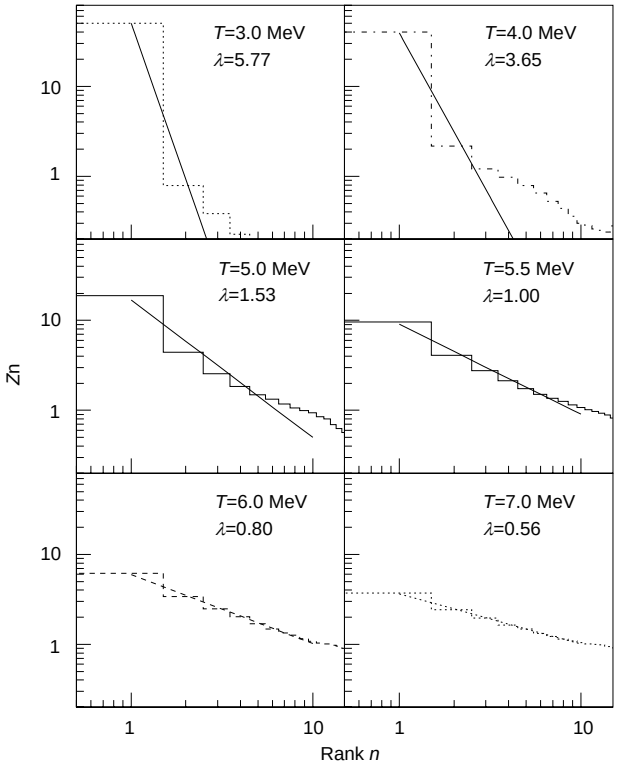

Fig.9 Zipf plots for T=3~7 MeV with LGM calulation. The dots are data and the lines are power-law fits (Eq.10). From Ref.[65].

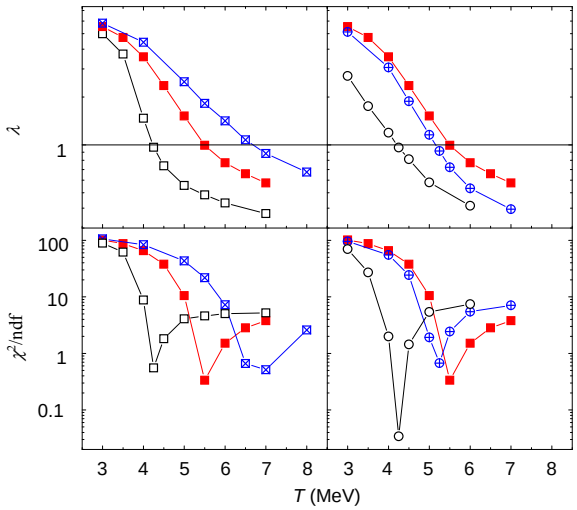

Fig.10 The slope parameter λ of the relation A_n to n (upper panel) and the χ^2/ndf with the fit of Zipf's law (lower panel) as a function of temperature. Left panel is the LGM results with differentρ_f (open squares: 0.18ρ_0, solid squares: 0.38ρ_0 and squares with cross: 0.60 ρ_0) and right panel is the comparisons of MD (open circles: MD with Coulomb force and circles with cross: MD without Coulomb) to LGM (solid squares) with 0.38 ρ_0.From Ref. [16].

holds (λ=1), for each calculation case. For the LGM case, the phase transition temperature increases with the freeze-out density; for the MD (i.e. CMD) case, a slight small transition temperature is obtained when Coulomb force is ignored. It becomes much lower in

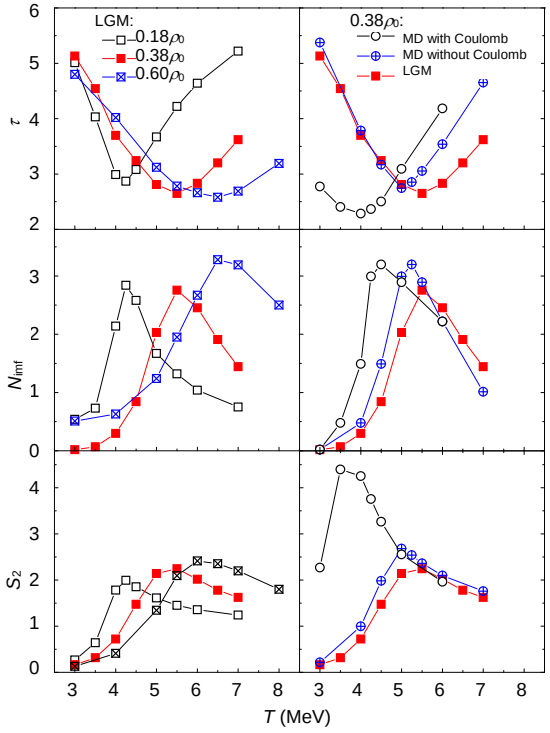

Fig.11 The effective power-law parameter, τ, the second moment of the cluster distribution, S_2, and the multiplicity of intermediate mass fragments, N_{imf}, as a function of temperature for the disassembly of ^{129}Xe. Left panel is the LGM results with differentρ_f and right panel is the comparison of MD to LGM with 0.38 ρ_0. From Ref.[16].

case of Coulomb interaction due to its long range repulsion.

Now we return to the TAMU data.[58] As shown in Fig.4, the region of 5~6 MeV/nucleon excitation energy is thought to be related to the liquid gas phase transition. The significance of this region in our data is further indicated by a Zipf's law analysis. Fig.12 shows the Zipf plots in nine excitation energy windows. The Zipf-law parameters λ are also extracted and shown in Fig.13. This rank ordering of the probability observation of fragments of a given atomic number, from the largest to the smallest, does indeed lead to a Zipf's law parameter λ~1 in the 5~6 MeV/nucleon range.

In a recent analysis for multifragment emission for CERN EMU13 data, Dabrowska *et al*. analyze emulsion data for 158 A GeV Pb-Pb and Pb-Plastic collisions and tested our Zipf law.[69] They found that their data are roughly consistent with the nuclear Zipf law. This may be interpretated as an evidence for the existence of the critical temperature associated with a liquid gas phase transition.[69] More recently, we applied the Zipf law to the mesons and baryons which

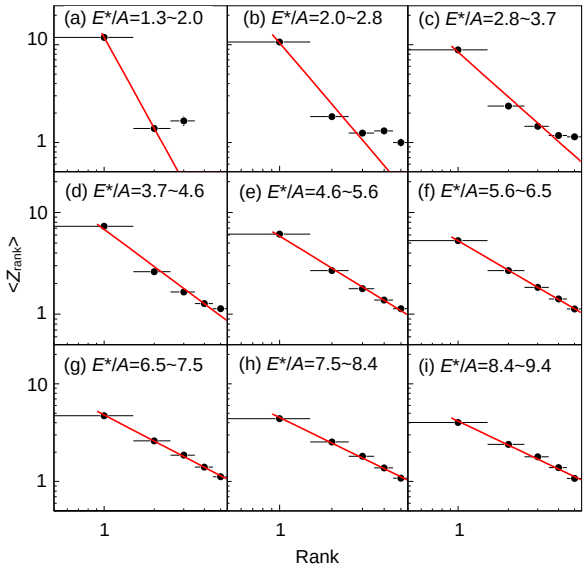

Fig.12 Zipf plots in nine different excitation energy bins. The dots are data and the lines are power-law fits (Eq.10). From TAMU data.[58]

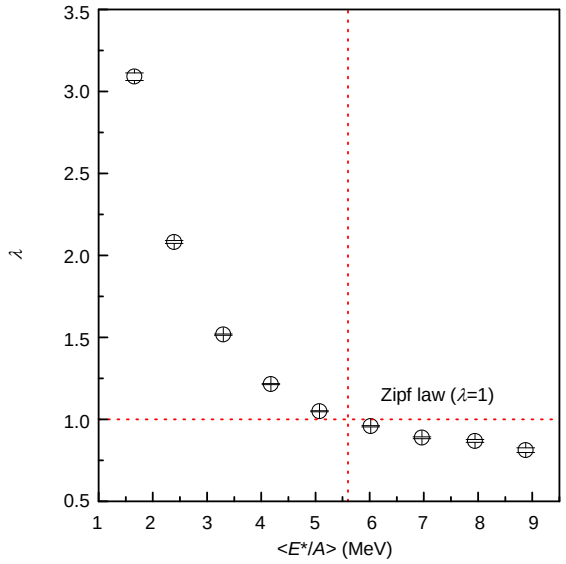

Fig.13 Zipf parameter as a function of excitation energy in TAMU data.[58]

are produced in the relativistic heavy ion collision. Some preliminary results are also obtained.[70]

In a related observation which is consistent with the formulation of Zipf's law, percolation model calculations[71] suggest that the ratio $S_p = \frac{\langle Z_{2\,\max}\rangle}{\langle Z_{\max}\rangle}$ reaches 0.5 around the phase separation point. Here $Z_{2\max}$ is the atomic number of the second heaviest fragment in each event. Fig.14 shows S_p versus E^*/A for TAMU data. S_p=0.5 near 5.5 MeV/nucleon and exhibits essentially linear behavior (with two different slopes) above and below that point, which also supports the onset of a phase change around that point.

If we make a plot for the average value of $Z_{2\max}$ vs $Z_{\max}$ in the nine excitation energy windows, we immediately see that a transition occurs between 5~6 MeV/nucleon (Fig.15). Below 5 MeV/nucleon of excitation energy, $\langle Z_{2\max}\rangle$ increases with increasing $\langle Z_{\max}\rangle$. In this energy zone, the fragmentation is basically dominated by evaporation and sequential decay is important. But above 6 MeV/nucleon excitation energy, $\langle Z_{2\max}\rangle$ decreases with increasing $\langle Z_{\max}\rangle$. In

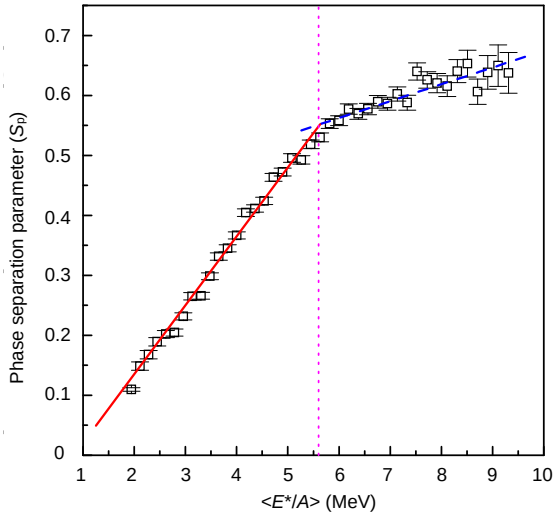

Fig.14 The phase separation parameter as a function of excitation energy in TAMU data.[58]

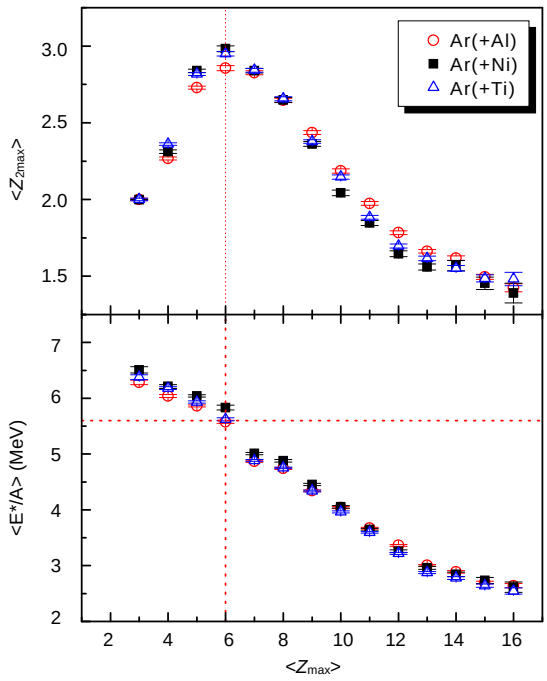

Fig.15 $\langle Z_{2\max}\rangle$ as a function of $\langle Z_{\max}\rangle$ in TAMU data.[58] The mean excitation energy is also shown.

this region of excitation, the nucleus is essentially fully vaporized and each cluster shows a similar behavior.

In relating theoretical calculation with I-CMD for $A \leqslant 36$,[58] we obtain the very similar pictures as the data. Fig.16 shows the scattering plots for Z_{2max} and Z_{max} for temperature $T = 3$ to 8 MeV. An obvious transition of the behavior occurs around 5.0 MeV, namely from the negative correlation to positive correlation, which inflects the phase transition point.[72] Of course, in I-CMD simulation, the input parameter is temperature instead of the excitation energy which can be determined from the data. However, the qualitative results are very similar.

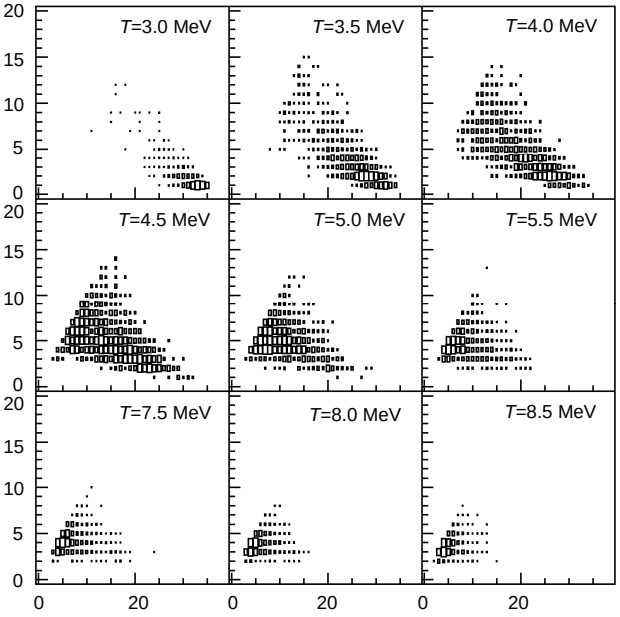

Fig.16 The scattering plots for Z_{2max} and Z_{max} in nine different temperature windows in I-CMD simulation. The y-axis is for Z_{2max} and x-axis for Z_{max}. From Ref.[58].

3.5 Bimodality

Another proposed test of phase separation is bimodality which was suggested in [73]. As has been noted,[74] this approach generalizes definitions based on curvature anomalies of any thermodynamic potential as a function of an observable which can then be seen as an order parameter. It interprets a bimodality of the event distribution as coexistence, each component representing a different phase. It provides a definition of an order parameter as the best variable to separate the two maxima of the distribution. In this framework when a nuclear system is in the coexistence region, the probability distribution of the order parameter is bimodal.

In analyses of INDRA data,[74] the bimodality parameter is defined as

$$P = \frac{\sum_{Z_i \geqslant 13} Z_i - \sum_{3 \leqslant Z_i \leqslant 12} Z_i}{\sum_{Z_i \geqslant 3} Z_i} \qquad (11)$$

P was chosen as a sorting parameter which may be connected with the density difference of the two phases ($\rho_l - \rho_g$), which is the order parameter for the liquid gas phase transition. Fig.17 shows the event distributions observed at different incident energies. These results show that none of the distributions is Gaussian, which would indicate a pure phase, but the gas phase part is dominant above 45 MeV/nucleon, while the liquid part is more important below 32 MeV/nucleon. Two components are roughly equal around 39 MeV/nucleon. The observed trends are relevant to the liquid gas phase transition.

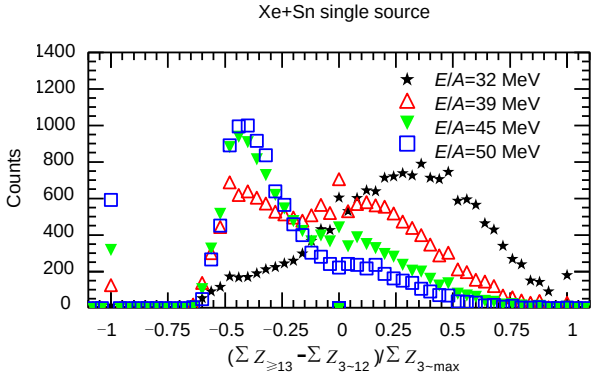

Fig.17 Event distributions observed at different incident energies. Points located at the values -1 are divided by 10. See text for the variable used for event distribution. From INDRA data.[74]

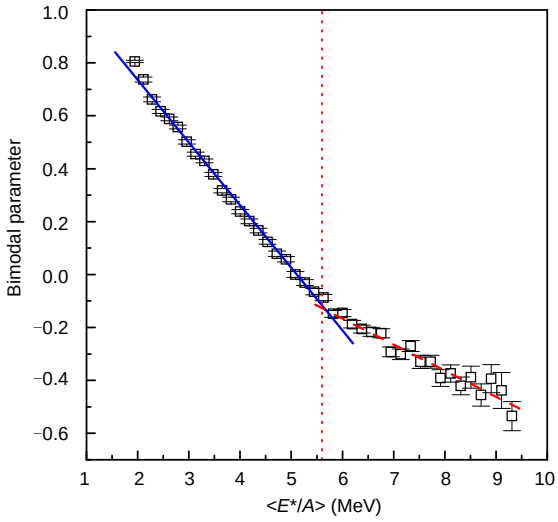

Fig.18 The average value of bimodality parameter as a function of excitation energy. From TAMU data.[58]

For our TAMU data for very light system, if we consider the clusters with $Z\leqslant 3$ as a gas and the clusters with $Z\geqslant 4$ as a liquid, a parameter characterizing the bimodal nature of the distribution can be defined as

$$P=\frac{\sum_{Z_i\geqslant 4}Z_i-\sum_{Z_i\leqslant 3}Z_i}{\sum_{Z_i\geqslant 1}Z_i} \tag{12}$$

Fig.18 shows the mean value of P as a function of E^*/A. Here again, the slope shows a distinct change at E^*/A = 5~6 MeV where P=0, i.e. the point of equal distribution of Z in the two phases.

3.6 Multiplicity information entropy

The concept of multiplicity information entropy has been also introduced into the diagnosis of nuclear liquid gas phase transition recently.[16] Originally, the information entropy was defined by Shannon in information theory[75] and it measures the "amount of information" which is contained in messages sent along a transmission line. It can be expressed as

$$H=-\sum_i p_i \ln p_i \tag{13}$$

where p_i is a normalized probability, and $\sum_i p_i=1$. Jaynes proposed that a very general technique for discovering the least biased distribution of the p_i consists in the maximization of the Shannon H entropy, subject to whatever constraints on p_i are appropriate to the particular situation. The maximization of H was thus put forward as a general principle of statistical inference-one which could be applied to a wide variety of problems in economics, engineering and many other fields, such as quantum phenomena.[75] In high energy hadron collisions, multiparticle production proceeds on the maximum stochasticity, i.e. they should obey the maximum entropy principle. This kind of stochasticity can be also quantified via the information entropy which has been shown to be a good tool to measure chaoticity in hadron decaying branching process.[76] In different physical conditions, information entropy can be expressed with different stochastic variables. In this work on HIC, we define p_i as the event probability of having "i" particles produced, i.e. $\{p_i\}$ is the normalized probability distribution of total multiplicity, the sum is taken over whole $\{p_i\}$ distribution. This emphasis is on the event space rather than the phase space. As shown below this kind of information entropy can be taken as a method to determine nuclear liquid gas phase transition.

Fig.19 shows the information entropy for disassembly of Xe.[16] The information entropy exhibits a rise and fall with temperature, which is similar to the behaviors of $N_{\rm imf}$ and S_2 (see Fig.11). The temperatures extracted from the peak values of H are consistent with the transition temperatures in Fig.1, indicating that information entropy ought to be a good diagnosis of phase transition. Physically, the maximum of H reflects the largest fluctuation of the multiplicity probability distribution in the phase transition point. In this case it is the most difficult to predict how many clusters will be produced in each event, i.e. the disorder (entropy) of information is the largest. Generally speaking, the larger the dispersal of multiplicity probability distribution, the higher the information entropy and then the disorder of system in the event topology. One should make a careful distinction between this information entropy, on the one hand, and the original thermodynamic entropy, on the other hand.[75] The latter generally illustrates the heat disorder in momentum space rather than event space and it always increases with temperature.

More recently, we have applied the same multiplicity information entropy to the relativistic heavy ion collision already.[77]

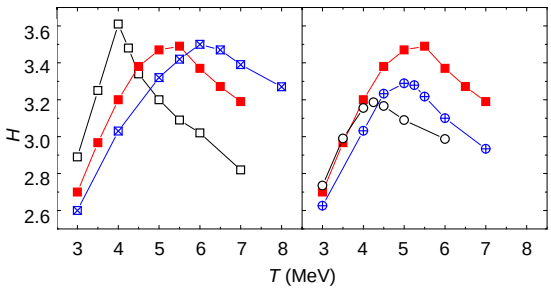

Fig.19 Information entropy H as a function of temperature. The symbols are the same as in Fig.11. From Ref.[16].

3.7 Campi plots

One of the well known characteristics of the systems undergoing a continuous phase transition is the occurrence of the largest fluctuations. These large fluctuations in cluster size and density of the system arise because of the disappearance of the latent heat at the critical point. In macroscopic systems such be-

havior gives rise to the phenomenon of critical opalescence.[78]

Campi suggested the use of event-by-event scatter plots of the natural log of the size of the largest cluster (here $\ln Z_{max}$) versus the natural log of the normalized second moment ($\ln S_2$) of the cluster distribution with the heaviest fragment removed,

$$S_2 = \frac{\sum_{Z_i \neq Z_{max}} Z_i^2 n_i(Z_i)}{\sum_{Z_i \neq Z_{max}} Z_i n_i(Z_i)} \quad (14)$$

where Z_i is the charge number of QP clusters and $n_i(Z_i)$ is the multiplicity of the cluster Z_i. As a means to observe the region of the largest fluctuations, such plots have proved to be very instructive in previous searches for critical behavior.[32]

In Fig.20 we present such plots for the nine selected excitation energy bins in our TAMU data. Again, in the low excitation energy bins of $E^*/A \leqslant 3.7$ MeV/nucleon, only the upper (liquid phase) branch exists, while at $E^*/A \geqslant 7.5$ MeV/nucleon, only the lower Z_{max} (gas phase) branch is strongly dominant. However, in the region of intermediate E^*/A of 4.6~6.5 MeV/nucleon, there appears to be a significant transition from the liquid dominated branch to the vapor branch, indicating that the region of maximal fluctuations signaling a transition between the two phases is to be found in that range.

As the Z_{max}–Z_{2max} correlation shown above, we obtain the similar Campi's plot with I-CMD simulation.[58] Fig.21 shows such plot. Similarly, the same transition is observed around 5.0 MeV indicating the onset of phase transition.

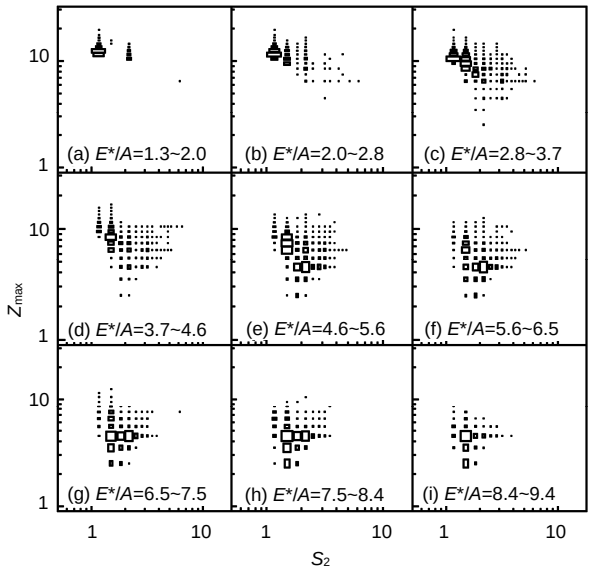

Fig.20 The Campi plot for different excitation energy windows. From TAMU data.[58]

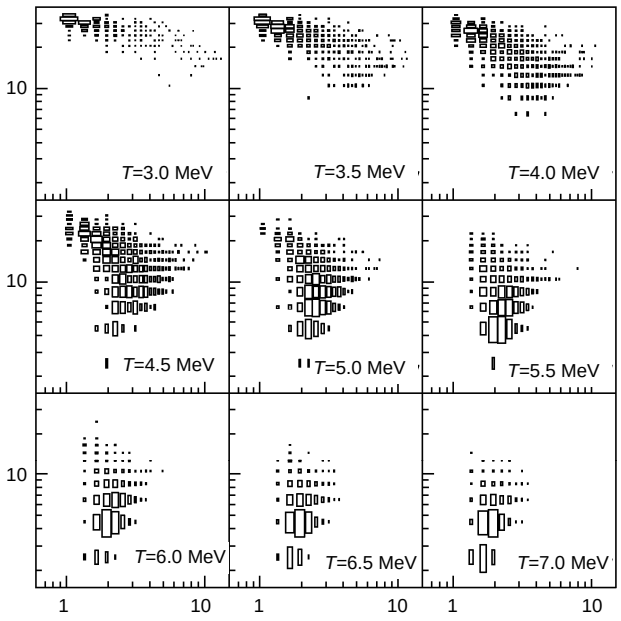

Fig.21 The Campi's plots for in nine different temperature windows in I-CMD simulation. The y-axis is for Z_{max} and x-axis for S_2. From Ref.[58].

Using the general definition of the kth moment as

$$M_k = \sum_{Z_i \neq Z_{max}} Z_i^k n_i(Z_i) \quad (15)$$

Campi also suggested that the quantity, γ_2, defined as

$$\gamma_2 = \frac{M_2 M_0}{M_1^2} \quad (16)$$

where M_0, M_1 and M_2, the zeroth moment, first moment and second moment of the charge distribution, could be employed to search for the critical region. In such an analysis, the position of the maximum γ_2 value is expected to define the critical point, i.e. the critical excitation energy E_c^*, at which the fluctuations in fragment sizes are the largest.

The excitation energy dependence of the average values of γ_2 obtained in an event-by-event analysis of our data is shown in Fig.22. γ_2 reaches its maximum in the 5~6 MeV excitation energy range. In contrast to observations for heavier systems,[79] there is no well defined peak in γ_2 for our very light system and γ_2 is relatively constant at higher excitation energies. We note also that γ_2 value is lower than 2 which is the expected smallest peak value for critical behavior if the system is large enough. However, 3D percolation studies indicate that finite size effects can lead to a

decrease of γ_2 with system size.[80,81] For a percolation system with 64 sites, peaks in γ_2 under two are observed. Therefore, the lone criterion γ_2>2 is not sufficient to discriminate whether or not the critical point is reached. To carry out further quantitative explorations of maximal fluctuations we have investigated several other proposed observables expected to be related to fluctuations and to signal critical behavior. These are discussed below.

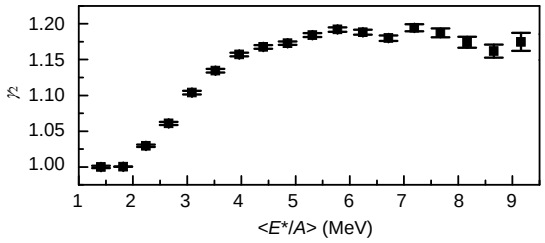

Fig.22 γ_2 of the QP system formed in Ar+Ni as a function of excitation energy. From TAMU data.[58]

3.8 Fluctuations in the distribution of Z_{max}

It is supposed that the cluster size distributions should manifest the maximum fluctuations around the critical point where the correlation length diverges. As a result of constraints placed by mass conservation, the size of the largest cluster should then also show large fluctuations.[78] Thus, it has been suggested that a possible signal of critical behavior is the fluctuation in the size of the maximum fragment.[32] Recently, Dorso *et al*. employed a molecular dynamics model to investigate fluctuations in the normalized variance (*NVZ*),

$$NVZ = \frac{\sigma^2_{Z_{\max}}}{< Z_{\max} >} \tag{17}$$

of the atomic number of the heaviest fragment (Z_{max}).[82] They found that this quantity can indeed display a maximum in the critical region.

In their work, Dorso *et al*. performed calculations of the *NVZ* on two simple systems, one of which should not exhibit critical behavior and the other does. For the first they used a random partition model, in which the population of different mass numbers is obtained by randomly choosing values of A following a previously prescribed mass distribution.[83] In this case the fluctuations in the populations are of statistical origin or are related to the fact that the total mass A_{tot} is fixed. No signal of criticality is to be expected. In the second case they explored the disassembly of systems of the same size employing a finite lattice bond percolation model. Such a case is known to display true critical behavior. They found that *NVZ* peaks close to the critical point in the percolation model calculation but shows no such peak in the random partition model calculation. This indicates that the mass conservation criterion, by itself, can not induce the peak of *NVZ*. The details can be found in [82].

For our TAMU data we plot the normalized variance of Z_{max} as a function of excitation energy in Fig.23. A clear maximum, characterizing the largest fluctuation of this order parameter, is seen, which is located around E^*/A=5~6 MeV/nucleon.

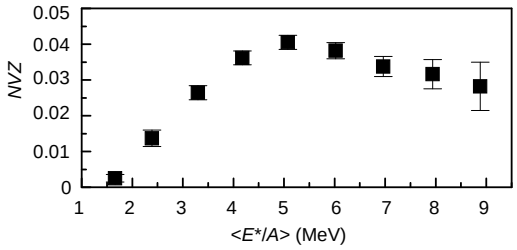

Fig.23 *NVZ* of the QP system formed in Ar+Ni as a function of excitation energy in our TAMU data.[58]

3.9 Fluctuations in the distribution of total kinetic energy and negative heat capacity

The system we have studied is a hot system. If critical behavior occurs, it should also be reflected in large thermal fluctuations. Using a definition similar to that of the normalized variance of Z_{max}, we can define the normalized variance of total kinetic energy per nucleon,

$$NVE = \frac{\sigma^2_{E^{\rm tot}_{\rm kin}/A}}{< E^{\rm tot}_{\rm kin} / A >} \tag{18}$$

where $E^{\rm tot}_{\rm kin} / A$ is the total kinetic energy per nucleon and $\sigma_{E^{\rm tot}_{\rm kin}/A}$ is its width. Fig.24 shows the *NVE* as a function of excitation energy in TAMU data. The observed behavior is very similar to that of *NVZ*. Again, the maximal fluctuation was found at E^*/A=5~6 MeV/u. The maximal thermal fluctuations are found in the same region as the maximal fluctuations in the largest cluster sizes.

The use of kinetic energy fluctuations as a tool to measure microcanonical heat capacities has also been proposed.[84-87] It has been shown[84] that for a given total energy the average partial energy stored in a subsystem of the microcanonical ensemble is a good

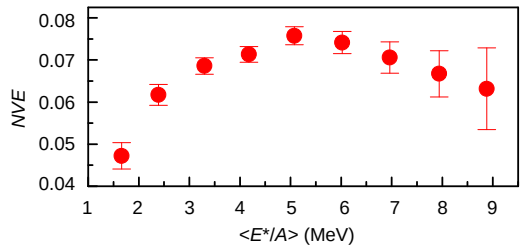

Fig.24 *NVE* of the QP system formed in Ar+Ni as a function of excitation energy in our TAMU data.[58]

thermometer while the fluctuations associated to the partial energy can be used to evaluate the heat capacity. An example of such a decomposition is given by the kinetic energy E_k and the interaction energy E_I. The interaction energy fluctuation can then be studied as a function of the total energy and the heat capacity, and can be evaluated according to

$$C = \frac{C_k^2 T^2}{C_k T^2 - \sigma_k^2} \tag{19}$$

where $\sigma_k^2 = \sigma_I^2$ is the fluctuation of the interaction energy E_I, T is the temperature, and C_k is the kinetic heat capacity that can be evaluated by taking the numerical derivative of $<E_k>=E^*-<E_I>$ with respect to T. Eq.(19) shows that a negative heat capacity corresponds to partial energy fluctuations in the microcanonical ensemble that exceed the corresponding fluctuations in the canonical ensemble ($\sigma_{can}=C_k T^2$).

In particular, first order phase transitions are marked by singularities and negative heat capacities,[35,84] corresponding to fluctuations anomalously larger than the canonical expectation. If the system is in statistical equilibrium, a measurement of anomalous fluctuations at a given energy is an unambiguous proof of a thermal first order phase transition. Fig.25 shows the normalized partial energy fluctuations and

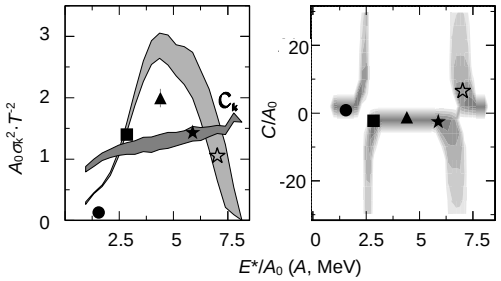

Fig.25 Left panel: normalized partial energy fluctuations and kinetic heat capacity for QP events (grey contours) and central Au+C (black dots), Au+Cu (squares, triangles), Au+Au reactions before (open stars) and after subtraction of 1 *A* MeV radial flow (black stars). Right panel: heat capacity per nucleon of the source for QP events and central reactions. From Ref.[87].

kinetic heat capacity for QP events (grey contours) and central Au+C (black dots), Au+Cu (squares, triangles), Au+Au reactions before (open stars) and after subtraction of 1 *A* MeV radial flow (black stars).

3.10 Universal fluctuations: Δ-scaling

The recent developed theory of universal scaling laws of order-parameter fluctuations provides a method to select order parameters and characterize critical and off-critical behavior, without any assumption of equilibrium.[88] In this framework, universal Δ-scaling laws of the normalized probability distribution $P[m]$ of the order parameter m for different "system size" $<m>$, should be observed:

$$< m >^{\Delta} P[m] = \Phi(Z_{(\Delta)}) \equiv \Phi[\frac{m - m^*}{< m >^{\Delta}}] \tag{20}$$

with $0 \leqslant \Delta \leqslant 1$, where $<m>$ and m^* are the average and the most probable values of m, respectively, and $\Phi(z_{(\Delta)})$ is the (positive) defined scaling function which depends only on a single scaled variable $Z_{(\Delta)}$. If the scaling framework holds, the scaling relation is valid independently of any phenomenological reasons for changing $<m>$.[88] The Δ-scaling analysis is very robust and can be studied even in small systems if the probability distributions $P[m]$ are known with a sufficient precision.

Botet *et al*. introduced this universal scaling method to the INDRA data for ^{136}Xe+^{124}Sn collisions in the range of bombarding energies between 25 MeV/nucleon and 50 MeV/nucleon. They chose the largest fragment charge, Z_{max}, as the order parameter. It was found that at $E_{lab} \geqslant 32$ MeV/nucleon, there is a transition in the fluctuation regime of Z_{max} which is compatible with a transition from the ordered phase with $\Delta = 1/2$ scaling to the disordered phase with $\Delta = 1$ scaling of excited nuclear matter.[15] From this study, they attributed the fragment production scenario to be in the family of aggregation scenarios which contains both equilibrium models such as the Fisher droplet model, the Ising model, or the percolation model and off-equilibrium models such as the Smoluchowski model of gels. For such scenarios the average size of the largest cluster, $<Z_{max}>$, is the order parameter and the cluster size distribution at the critical point obeys a power law with $\tau>2$.

We have applied the same technique to the Z_{max} distribution from our TAMU data. Fig.26(a) shows the Δ-scaling features of $P[Z_{max}]$ distributions for ^{40}Ar+^{58}Ni collisions in different excitation energywindows.

The upper panel shows that Δ-scaling of $P[Z_{max}]$ distributions for all E^*/A windows above 2.0 MeV with $\Delta=1$. Essentially for this $\Delta=1$ scaling the curves at higher excitation energy above 5.6 MeV/nucleon can be compressed into a single curve, however, the curves of lower E^*/A deviate from this first-scaling (i.e. $\Delta=1$). This situation of lower E^*/A curves disappears when $\Delta=1/2$ scaling was used. Fig.26(b) shows the curves with $\Delta=1/2$. Now these curves collapse onto one curve, i.e. they obey $\Delta=1/2$ scaling, but in this case, the scaling curves for higher E^*/A which obeys $\Delta=1$ scaling as shown in Fig.26(a) becomes worse and deviate from lower E^*/A curves. For comparison, Fig.26(c) only plot the higher E^*/A scaling curves with $\Delta=1$ and the lower E^*/A scaling curves with $\Delta=1/2$. In this way, a transition from $\Delta=1/2$ scaling to $\Delta=1$ scaling was found in the region of E^*/A ~5.6 MeV for our light system. The latter scaling corresponds to the fluctuations of the Z_{max} growing

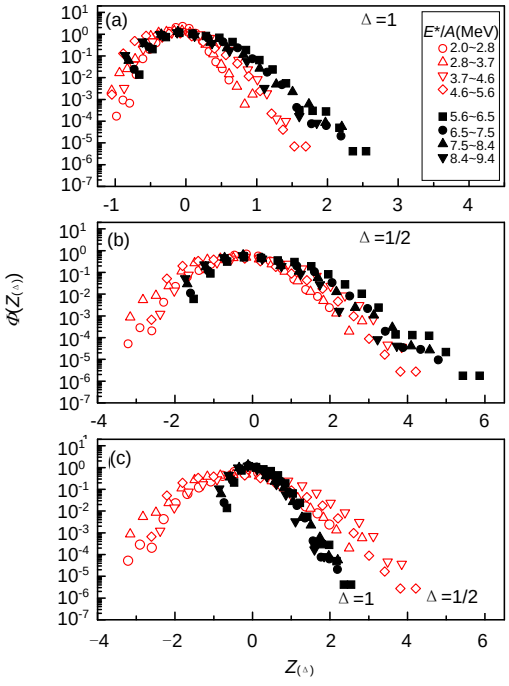

Fig.26 Δ-scaling for different E^*/A window: all E^*/A windows above 2.0 MeV/nucleon are shown together with $\Delta=1$ (a); same as (a) but with Δ=1/2 scaling (b); for four E^*/A windows above 5.6 MeV/nucleon with Δ=1 scaling and four E^*/A windows below 5.6 MeV/nucleon with $\Delta=1/2$ scaling (c). From TAMU data.[58]

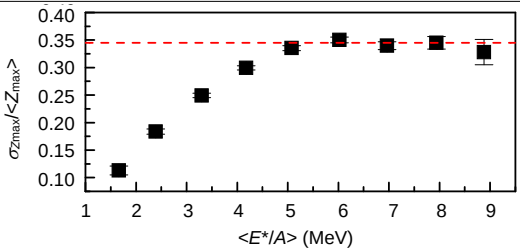

Fig.27 $\sigma/\langle Z_{max}\rangle$ as a function of $\langle E^*/A\rangle$. From TAMU data.[58]

with the mean value, i.e. $\frac{\sigma_{z_{max}}}{<z_{max}>}$~constant (see Fig.27). The saturation of the reduced fluctuations of Z_{max} (i.e. $\frac{\sigma_{z_{max}}}{<z_{max}>}$)observed above corresponds to the transition to the regime of maximal fluctuations.[89]

More recently, we have applied the Δ-scaling to multiplicity distribution, strange particle multiplicity and the number of binary nucleon-nucleon collision in CERN-SPS energy for p + p, C + C and Pb + Pb from 20 to 200 GeV/nucleon. It looks the scaling holds even in such high energy hadron transport process.[77]

3.11 Caloric curve

The caloric curve which relates the internal energy of an excited system at thermodynamic equilibrium to its temperature is a priori the simplest experimental tool to look for the existence of a phase transition. The first determination attempted by the ALADIN collaboration[6] collected the outcome of ^{197}Au on ^{197}Au collisions at 600 MeV/nucleon with data obtained by means of less energetic collisions. The excitation energy was determined by following the procedure prescribed in Ref. [90] and the corresponding temperature fixed by means of arguments relating this quantity to the so called double ratio procedure,[91] in the present case the ratios of ^{3}He/^{4}He and ^{6}Li/^{7}Li isotopes. The corresponding curve showed the features of a rather strong first order transition, with a characteristic close to constant temperature T over a large energy interval lying between 3 and 10 MeV excitation energy per nucleon, which may be interpreted as a sign for the generation of latent heat and followed by a strong increase of T with excitation energy above 10 MeV. However, a critical discussion followed this observation, in which the hypotheses and simplifications underlying the definition of the temperature, the freeze-out density and the increase of T at high excitation energy were examined.[92]

Ma *et al*. measured Ar on Ni collisions at 52 and 95 MeV/nucleon with the 4π multi-detector (INDRA) in order to investigate this point.[93] Several double isotopic yield ratios were used in order to define the temperature. We led to different apparent slope temperature increase as a function of the excitation energy. The issue of the experiment and its interpretation have been performed by means of statistical models.[94-96] A temperature plateau is absent for such a light system.

In our TAMU data the caloric curve is also constructed.[58] Quasi-projectile has been reconstructed with a new method.[59] The determination of initial temperature has been deduced by taking the cascade method for lower excitation energies[97] or quantum statistical model correction for higher excitation energies[96,98] into account. Fig.28 shows the resultant caloric curve of quasi-projectile Ar. Based upon the fluctuation data and Fisher power law analysis of our TAMU data, the corresponding initial temperature around the critical point is 8.3 ± 0.5 MeV in the region of 5.5 MeV/nucleon excitation energy.

More measurements for the caloric curves have been performed in various groups. For instance, for 100 MeV/nucleon Au+C from EOS group, 4.8 GeV ^{3}He+Ag/Au reactions from ISIS group,[99] the excited systems with $A \leqq 110$ particles produced by means of different projectiles and targets with a bombarding energy of 47 MeV/nucleon[100] etc. Nuclear expansion density was also extracted from the analysis of caloric curves.[101] A collection of the experimental data for the caloric curves has been used to deduce the critical temperature as shown in the following section.

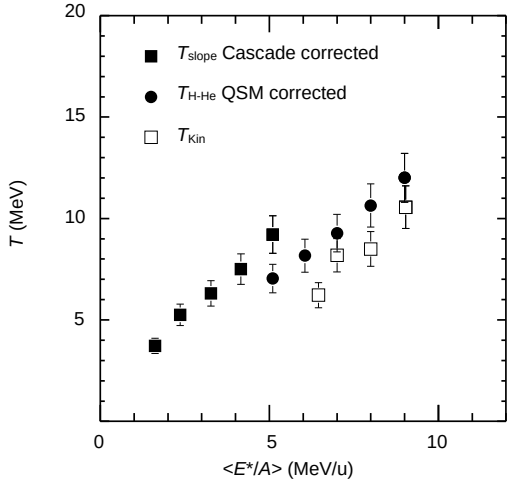

Fig.28 The deduced caloric curves for Ar quasi-projectiles ($A \leqq 36$) in TAMU data.[58]

3.12 Critical temperature

We collected the experimental data for caloric curve in terms of different mass windows and found that the onset temperature of the temperature plateau, so-called the limiting temperature ($T_{\rm lim}$), shows the dropping trends with the system mass.[102] See Fig.29. This reflects the influence of the Coulomb interaction on nuclear instability. In a recent theoretical calculation, Li *et al*. also shows the limiting temperatures decrease with the increasing of mass number for nuclei along the β-stability line,[103] which is in agreement with the earlier results of Song and Su *et al*.[104,105]

Mean values of $T_{\rm lim}/T_{\rm c}$ for five different masses which result from averaging the results of different calculations[104-113] are shown in Fig.30. The estimated uncertainties are relatively small, ≈6%. For comparison, the figure also presents ratios of $T_{\rm lim}/T_{\rm c}$ which are expected to result assuming only finite size effects as derived from a lattice calculation[114] and the ratio of the nuclear binding energy per nucleon along the line of beta stability to the bulk binding energy per nucleon, 16 MeV. We have employed the mean variation of $T_{\rm lim}/T_{\rm c}$ with A, determined from commonly used microscopic theoretical calculations, together with the five experimental limiting temperatures reported in Ref. [7], to extract the critical temperature of nuclear matter. In doing so we treat the theoretical variation as if it were an experimental uncertainty. Since the various interactions employed have been "tuned" to other nuclear properties, we consider this a reasonable approach. The results are presented

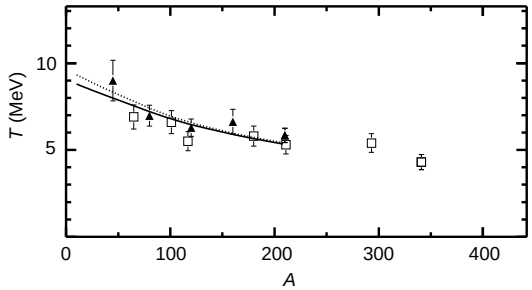

Fig.29 Limiting temperatures vs mass. Limiting temperatures derived from double isotope yield ratio measurements are represented by solid triangles. Temperatures derived from thermal bremasstrahlung measurements are represented by open squares. Lines represent limiting temperatures calculated using interactions proposed by Gogny (dashed)[108] and Furnstahl *et al* (solid).[105] From Ref.[102].

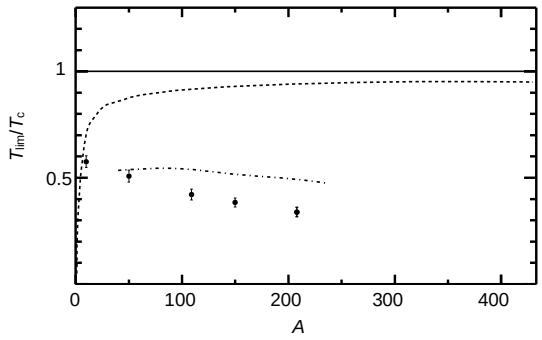

Fig.30 Theoretical variation of the ratio T_{lim}/T_c with mass along the line of beta stability. The solid line indicates the reference value of T_c. The short dashed line shows the effect of finite size scaling derived from an Ising mode.[114] The line with alternating short and long dashes depicts the ratio of the nuclear binding energy per nucleon to the bulk binding energy per nucleon, 16 MeV. Points with uncertainties are derived from the model calculations in Ref. [104]~[113]. From Ref.[102].

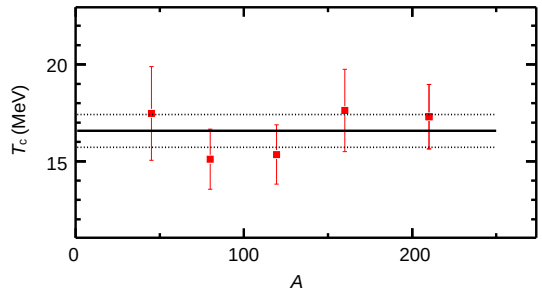

Fig.31 Derived values of the critical temperature of symmetric nuclear matter. Values derived from data in five different mass regions are presented. The mean value of 16.6 MeV is indicated by the horizontal solid line. The range corresponding to ± one standard deviation from this mean value is shown by the thin dotted lines. From Ref. [102].

in Fig.31. Averaging the individual results we find 16.6 ± 0.86 MeV.

This has been used to derive both K, the incompressibility and m^*, the effective mass. Extracted by comparison with the same interactions as were employed to determine K from observations of the Giant Monopole Resonance at low excitation energy, the value of K, obtained here from properties of nuclei at moderate excitation energies, is found to be in excellent agreement with that GMR result.[115]

The critical temperature has been also extracted by the IMF charge distribution for p+Au collisions at 8.1 GeV within the Statistical Multifragmentation Model with T_c (at which surface tension vanishes) as a free parameter.[116,117] The value T_c=20 ± 3 MeV (90% CL) obtained from the best fit to the data is considered as an effective value of the critical temperature averaged over all the fragments produced in the collision. This value is significantly larger than those found in Ref.[18] by the analysis of the multifragmentation data in terms of Fisher's droplet formalism. A surprisingly large range of T_c values in different publications indicates severe model dependence of the results. Although the SMM value for T_c is model dependent, as is any other estimate of the critical temperature, the analysis presented here provides strong support for a value of T_c>15 MeV.

3.13 Phase coexistence diagram

Recently the phase coexistence curve of finite neutral nuclear matter has been constructed from the EOS multifragmentation data of gold, lanthanum and krypton nuclei obtained. The fragment yields are examined in terms of Fisher's droplet formalism modified to account for Coulomb energy. The critical exponents σ and τ and the surface energy coefficient c_0 are obtained. Estimates are made of the pressure-temperature and temperature-density coexistence curve of finite neutral nuclear matter as well as the location of the critical point.

In the analysis of Elliott *et al*.,[19] the reduced density is given by

$$\frac{\rho}{\rho_c} = \frac{\sum A_{n_A}(T)}{\sum A_{n_A}(T_c)} \tag{21}$$

where A is cluster mass and n_A is its multiplicity. T is temperature and T_c is critical temperature. Eq.21 gives the low density (vapor) branch of the coexistence curve of finite nuclear matter, shown in Fig.32.

Following Guggenheim's work with simple fluids, it is possible to determine the high density (liquid) branch as well: empirically, the ρ/ρ_c-T/T_c coexistence curves of several fluids can be fit with the function:[118]

$$\frac{\rho_{l,v}}{\rho_c} = 1 + b_1\left(1 - \frac{T}{T_c}\right) \pm b_2\left(1 - \frac{T}{T_c}\right)^{\beta} \tag{22}$$

where the parameter b_2 is positive (negative) for the liquid ρ_l (vapor ρ_v) branch. Using Fisher's formalism, β can be determined from τ and σ:[57]

$$\beta = \frac{\tau - 2}{\sigma} \tag{23}$$

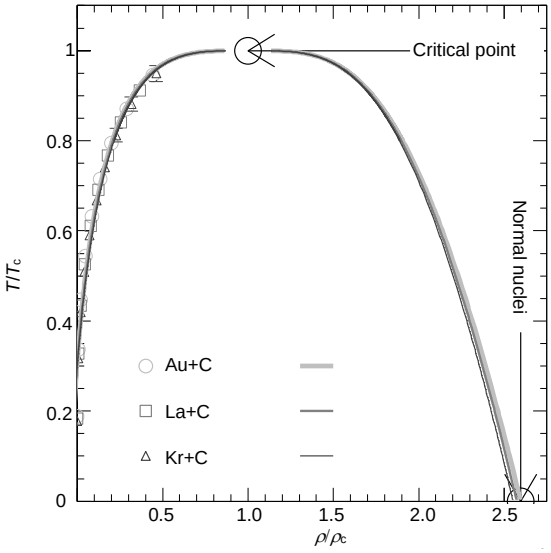

Fig.32 The points are calculations performed at the excitation energies below the critical point and the lines are a fit to and reflection of Guggenheim's equation. From Ref. [19].

For this work β=0.3±0.1. Using this value of β and fitting the coexistence curve from the EOS data sets with Eq.22 one obtains estimates of the ρ_v branch of the coexistence curve and changing the sign of β_2 gives the ρ_l branch, thus yielding the full T-ρ coexistence curve of finite nuclear matter.

From Fig.32 it is possible to make an estimate of the density at the critical point ρ_c. Assuming that normal nuclei exist at the T=0 point of the ρ_l branch of the coexistence curve, then using the parameterization of the coexistence curve in Eq.22 gives $\rho_c \sim \rho_0/3$.

3.14 Critical exponents

Since the pioneering work on extraction of the critical exponents for nuclear multifragmention from EOS data,[9] several additional experimental and theoretical efforts have been attempted.[119-121] In the latter works, Elliott *et al*. show that the scaling behavior can remain even in small systems and the critical exponents can be extracted.

In the Fisher droplet model, the critical exponent τ can be deduced from the cluster distribution near the phase transition point. In Sec.3.1, we already determined, from the yield distributions, $\tau_{\text{eff}} \sim 2.31 \pm 0.03$, which is close to that for the liquid gas phase transition universality class. In terms of the scaling theory, τ can also be deduced from S_{corr}, the slope of the correlation between lnS_3 vs lnS_2,[119] where $S_3 = M_3/M_1$, shown in Fig.33. S_{corr} is related to τ as

$$\tau = \frac{3S_{\text{corr}} - 4}{S_{\text{corr}} - 1} \tag{24}$$

Using the value of T_c=8.3 MeV determined from our caloric curve measurements (Fig.28), we take the values of S_2 and S_3 where the fragment with $Z_{\max}$ is excluded in the "liquid" phase but included in the "vapor" phase. The slopes were determined from linear fits to the "vapor" and "liquid" regions respectively and then averaged. In this way, we obtained a value of τ=2.15±0.1. See Fig.33.

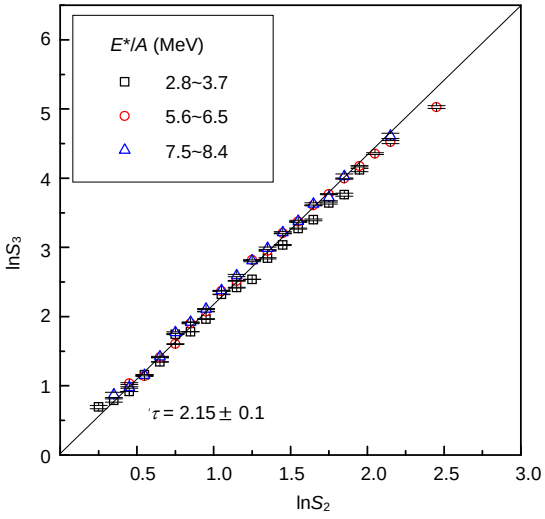

Fig.33 The correlation of lnS_3 vs lnS_2 and the linear fit. From TAMU data.[58]

Other critical exponents can also be related to other moments of cluster distribution, M_k, which were defined in Eq.15. Since, for our system, we have already deduced the initial temperatures and know the critical temperature T_c (8.3 MeV) at the point of maximal fluctuations, we can use temperature as a control parameter for such determinations. In this context, the critical exponent β can be extracted from the relation

$$Z_{\max} \propto (1 - \frac{T}{T_c})^{\beta} \tag{25}$$

and the critical exponent γ can be extracted from the second moment via

$$M_2 \propto \left| 1 - \frac{T}{T_c} \right|^{-\gamma} \tag{26}$$

In each case, $|1 - \frac{T}{T_c}|$ is the parameter which measures the distance from the critical point.

Fig.34 shows Z_{max} as a function of temperature. We note a dramatic change of Z_{max} around the critical temperature T_c. LGM calculations also predict that the slope of Z_{max} vs T will change at the liquid gas phase transition[53] (see Fig.6). Using the left side of this curve (i.e. liquid side), we can deduce the critical exponent β by the transformation of the x-axis variable to the distance from the critical point. Fig.34(b) shows the extraction of β with Eq.25. An excellent fit was obtained in the region away from the critical point, which indicates a critical exponent $\beta=0.33\pm0.01$. Near the critical point, the finite size effects become stronger so that the scaling law is violated. The extracted value of β is that expected for a liquid gas transition (See Table 1).[78]

To extract the critical exponent γ, we take M_2 on the liquid side without Z_{max} but take M_2 on the vapor side with Z_{max} included. Fig.35(a) shows lnM_2 as a function of $\ln(|1-\frac{T}{T_c}|)$. The lower points are from the liquid phase and the upper points from the vapor phase. For the liquid component, we use Eq.26 to obtain the critical exponent $\gamma=1.15\pm0.06$ from a good fit in a reasonable range of lnM_2. This value of γ is also close to the value expected for the liquid gas universality class (see Table 1). It is seen that the selected region has a good power law dependence.

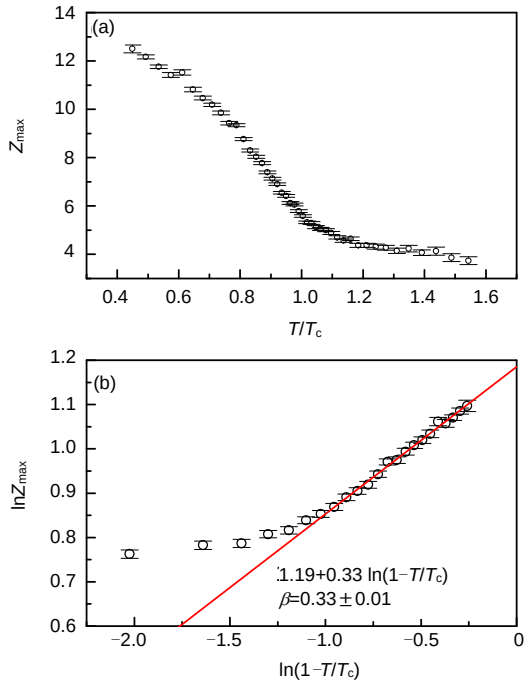

Fig.34 Z_{max} as a function of T/T_c (a) and the extraction of the critical exponent β (b). From TAMU data.[58]

Table 1 Comparison of the critical exponents

Exponents	3D percolation	Liquid-gas	This work
			2.22±0.46 (Eq.28)
τ	2.18	2.21	2.31±0.03 (Eq.9)
			2.15±0.10 (Eq.24)
β	0.41	0.33	0.33±0.01
γ	1.8	1.23	1.15±0.06
σ	0.45	0.64	0.68±0.04

However, a similar effort to extract the γ in the gas phase is not successful: a small value less than 0.20 is deduced. This may be due to the finite size effects for very light system. Since the largest cluster still exists in the vapor side, its inclusion (or exclusion) in M_2 might contaminate the true moment, this will result in an imprecise value of γ extracted from the vapor phase. For comparison, we just show, for the vapor phase, a line representing the γ derived from the liquid side. This line only agrees with the last few vapor points, i.e. the highest temperature points (the contamination of M_2 should the least there). In Fig.35(b) we also show M_2 as a function of $(1-\frac{T}{T_c})$. The left points are for vapor phase and right points for liquid phase and lines represent the same curves as in Fig.35. Again for the liquid phase, the critical exponent 1.15 shows an overall good fit, but for the gas phase it only describes the few points where the system has the highest temperatures.

Since we have the critical exponent β and γ, we can use the scaling relation

$$\sigma=\frac{1}{\beta+\gamma} \tag{27}$$

to derive the critical exponent σ. In such way, we get the $\sigma=0.68\pm0.04$, which is also very close to the expected critical exponent of a liquid gas system.

Finally, it is possible to use the scaling relation

$$\tau=2+\frac{\beta}{\beta+\gamma} \tag{28}$$

to check the τ value which was determined from the charge distributions using Fisher droplet model power law fits around the critical point (see Fig.3). Using Eq.28 we obtain $\tau=2.22\pm0.46$, which, though less

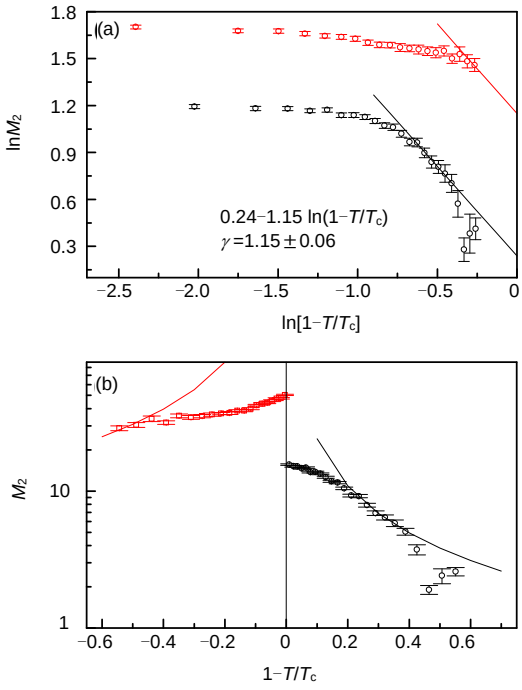

Fig.35 The extraction of critical exponents γ (a) and M_2 as a function of the distance from critical temperature (b). See text for details. From TAMU data.[58]

precise, is in good agreement with the values of 2.31 ±0.03 obtained from the charge distribution around the point of maximal fluctuations and 2.15±0.1 extracted from the correlation of lnS_3 vs lnS_2.

To summarize this section, we report in Table 1 a comparison of our results with the values expected for the 3D percolation and liquid gas system universality classes and with the results obtained by Elliott *et al*. for a heavier system. Obviously, our values for this light system with $A \leqq 36$ are consistent with the values of the liquid gas phase transition universality class rather than the 3D percolation class.

3.15 Spinodal instability

Recently the multifragmentation of very heavy fused systems formed in central collisions between ^{129}Xe and ^{nat}Sn at 32, 39, 45 and 50 A MeV with INDRA[122] has been studied.[14,123] These fused systems can be identified to well defined pieces of nuclear matter and eventually reveal fragmentation properties to be compared to models in which bulk instabilities are present.

Many theories have been developed to explain multifragmentation (see for example Ref.[20], [21], [124] for a general review of models). In particular, the concept of multifragmentation resulting from the volume instabilities of spinodal type has been proposed.[125] During a whole collision process, a wide zone of the nuclear matter phase diagram may be explored and the nuclear system may enter the liquid-gas low density phase coexistence region and even more precisely the unstable spinodal region. Therefore, a possible origin of multifragmentation may be found through the growth of density fluctuations in this unstable region. Within this theoretical scenario a breakup into nearly equal-sized "primitive" fragments should be favored in relation with the wave-lengths of the most unstable modes present in the spinodal region.[126] To search for such events a very sensitive correlation method was used, which is called "higher order correlations" and was proposed in Ref.[127]. The charge correlation is defined by the expression:

$$R = \left.\frac{Y(\Delta Z, < Z >)}{Y'(\Delta Z, < Z >)}\right|_M \qquad (29)$$

Here, $Y(\Delta Z, <Z>)$ is the yield of selected events with $<Z>$ and ΔZ values and M is the fragment multiplicity. The denominator $Y'(\Delta Z, <Z>)$ which represents the uncorrelated yield is built, for each fragment multiplicity, by taking fragments in different events of the selected sample. With such a correlation method, if events with nearly equal-sized fragments are produced, we expect to see peaks appearing at ΔZ values close to zero. Taking into account secondary decay of fragments, the bin ΔZ=0~1 was only considered. At 32 A MeV incident energy peaks were observed in this bin for each fragment multiplicity.[128,129] See Fig.36.

"Background" has been suitably constructed in order to estimate whether the enhancement of events with equal-sized fragments is statistically significant. Fig.36 shows the higher order correlation functions for the first bin in ΔZ with their statistical errors; the full line corresponds to the extrapolated "background". All events corresponding to the points whose error bar is fully located above this line correspond to a statistically significant enhancement of equal-sized fragment partitions. The number of significant events amounts to 0.1% of the selected fusion events.

The observed weak but unambiguous enhanced productions of events with equal-sized fragments at 32 and 39 A MeV can be interpreted as a signature of spinodal instabilities as the origin of multifragmenta-

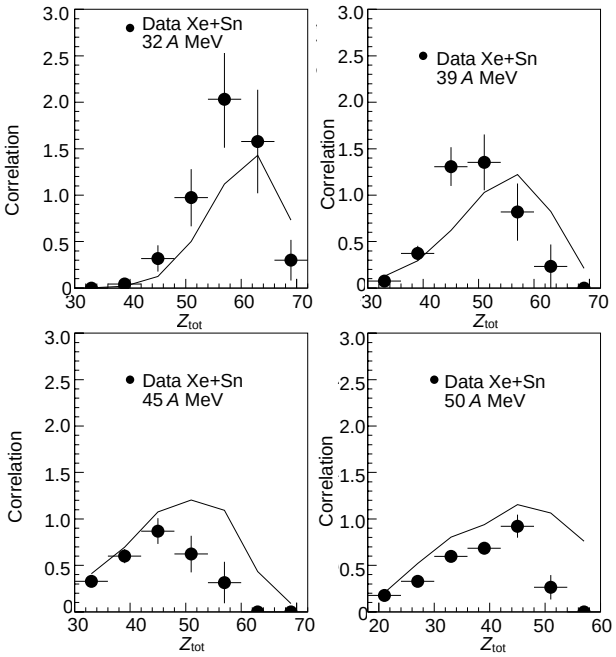

Fig.36 Higher-order charge correlations: quantitative results for experimental data at different incident energies. Symbols indicate the events where ΔZ=0~1, curves show the background (see text). Vertical bars correspond to statistical errors and horizontal bars define Z_{tot} bins. From Ref. [123].

tion in the Fermi energy domain. The observation is consistent with the measurement of negative microcanonical heat capacities for the same selected fused events at 32 A and 39 A MeV[130] which are predicted to sign a first order phase transition.[131]

3.16 Isospin effects

Since nuclei are composed of neutrons and protons, isospin effects may be very important for the nuclear liquid-gas phase transition.[132] As the asymmetry between neutron and proton densities becomes a local property in the system, calculations predict neutrons and protons to be inhomogenously distributed within the system resulting in a relatively neutron-rich gas and relatively neutron-poor liquid.[46,133,134] The critical temperature may also be reduced with increasing neutron excess reflecting the fact that a pure neutron liquid probably does not exist.[133] While our recent calculations suggest that the rather narrow range of isospin values available in the laboratory might not allow us to observe the decrease in critical temperature,[135,136] efforts are underway to study the fractionation of the isospin in the co-existence region.

In our calculation, we use I-LGM and I-CMD to investigate the isospin dependence of the apparent critical temperature for Xe-isotopes.[136] As discussed in Section 3.1, a minimum of power-law parameter τ_{min} exists if the critical behavior takes place. Fig.37(a) displays τ parameter as a function of temperature for Xe nuclei with the different isospin. The minimums of τ parameters in Fig.37(a) locate closely at 5.5 MeV for all the systems, which illustrates its minor dependence on the isospin. However, τ parameters show different values outside the critical region for nuclei with different isospin, e.g., τ decreases with isospin when T>5.5 MeV (multifragmentation region).

Fig.37(b) plots the information entropy H as a function of temperature for Xe isotopes. The information entropy H has peaks close to 5.5 MeV for all isotopes. These peaks indicate that the opening of the phase space in the critical point is the largest. In other words, the system at the critical temperature has the largest fluctuation/stochasticity which leads to the largest disorder and particle production rate. Beyond the critical point, the information entropy H increases with the isospin.

Similarly, Fig.37(c) gives the IMF multiplicity as a function of temperature for Xe isotopes. Again, the critical behavior occurs at the similar temperature, it has weak sensitivity to the isospin, as τ reveals.

In Fig.37(d) we give the temperature dependences of Campi's second moment of the fragment mass distribution.[33] At the percolation point S_2 diverges in an infinite system and is at maximum in a finite system. Fig.37(d) gives the maximums of S_2 around 5.5 MeV for different isotopes, respectively. Again, the critical behavior occurs at the same temperature, independent of the isospin, as τ reveals.

Based on the above analysis, it looks that the apparent critical temperature is very weak sensitive to the isospin of sources in the limited isospin range. This conclusion is not contradict with the previous studies on the isospin dependence of critical temperature like in [46], where the span of isospin is from symmetrical nuclear matter to pure neutron matter. If we only look a small span of isospin for the experimentally measurable medium size isotopes, like $^{122\text{-}146}$Xe, the change of critical temperature is neglect. This conclusion might indicate that it will be difficult

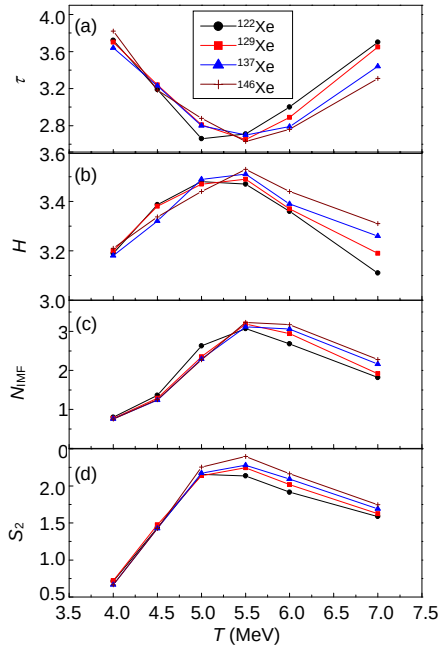

Fig.37 Critical observables: τ parameter from the power law fit to mass distribution (a), information entropy (b), multiplicity of IMF (c) and Campi's second moment (d) as functions of temperature and isospin of disassembling sources. From Ref.[136].

to search for the isospin dependence of critical temperature which signals the liquid gas phase transition for medium size nuclei in the experimental point of view. In addition, values of power law parameter of cluster mass distribution, mean multiplicity of intermediate mass fragments (IMF), information entropy (H) and Campi's second moment (S_2) also show minor dependence on the isospin of Xe isotopes at the critical point. In contrary, some isospin dependences of the values of τ, H, N_{IMF} and S_2 will reveal outside the critical region.

As the isospin effects are not large, the influence of sequential decays becomes important and may obscure the isospin fractionation effect one wishes to study. To minimize such problems, isobar pairs, such as (t, ^{3}He), which have the same number of internal excited states, have been used. Some indications for isospin fractionation are provided by the sensitivity of Y(t)/Y(^{3}He) distributions to the overall N/Z ratio of the system.[137] The ratios of Y(t)/Y(^{3}He) have also been observed to decrease with incident energies, in qualitative agreement with the predictions from the isospin dependent lattice gas model.[46,53,134,136] Light isobars such as (t, ^{3}He) pair may suffer from contamination of pre-equilibrium processes. Attempts have been made to use additional mirror isobar pairs such as (^{7}Li, ^{7}Be) and (^{11}B, ^{11}C)[138,139] and isospin fractionation was discussed.

4 Conclusions

In conclusion, theoretical background of nuclear liquid gas phase transition has been presented and extensive observables relating this kind of phase transition have been shown. When the nuclear liquid gas phase transition occurs, the fragment yield distribution obeys the power law which was predicted by Fisher droplet model. For intermediate mass fragments, their multiplicity rises to a maximum and then falls with the temperature or excitation. The emission rate of light particles and charged particles shows a turning point around the phase transition point. From fragment size structure, we found that there exists a particular hierarchical arrangement, so-called the nuclear Zipf-type law, which was supported by both the calculation of lattice gas model and Texas A&M data and EMU13 CERN data. The scattering plots of the correlation between Z_{max} and Z_{2max} shows a significant transition around the phase transition point. Bimodality parameter also gives a phase separation between dominant liquid phase and dominant gas phase when phase transition takes place.

Besides, many observables demonstrate the existence of maximal fluctuations when phase transition occurs. These fluctuation observables include the Campi scattering plots and the normalized variances of the distributions of order parameters, Z_{max} and total kinetic energy and related heat capacity. Δ-scaling analysis also shows a universal behavior at higher excitation energy where the saturation of the reduced fluctuations of Z_{max} (i.e. $\frac{\sigma_{z_{max}}}{< z_{max} >}$) is observed. This corresponds to the transition to the regime of large fluctuations from the ordered phase at lower excitation energy.

Caloric curves, critical temperature, critical exponents, phase co-existence diagram and spinodal instability are also discussed. All of them can provide some useful information on liquid gas phase transition.

Before the end of this review, we should keep in mind that a vast amount of work has been done in this field by groups spread world-wide. The literature on

this subject is enormous. Our review report had to be necessarily selective. Some interesting works must have left out, we apologize for all the omissions that occurred.

Acknowledgments

We appreciate many helpful discussions with colleagues and/or friends, especially Joe Natowitz, Jean Péter, Bernard Tamain, Subal Das Gupta, Jicai Pan, Manyee Betty Tsang and Bao-an Li, Roy Wada, Kris Hagel, Sherry Yennello *et al*.

References

1 Lynden-Bell B. Physica **A**, 1999, **263**: 293
2 Bertsch G F. Science, 1997, **277**: 1619
3 Finn J E *et al*. Phys Rev Lett, 1982, **49**: 1321
4 Rivet M F *et al*. Phys Lett **B**, 1996, **388**: 219
5 Gross D H E. Rep Prog Phys, 1990, **53**: 605 and references therein
6 Pochodzalla J *et al*. Phys Rev Lett, 1995, **75**: 1040
7 Natowitz J B *et al*. Phys Rev **C**, 2002, **62**: 034618
8 Bondorf J P *et al*. Phys Rev **C**, 1998, **58**: R27
9 Gilkes M L *et al*. Phys Rev Lett, 1994, **73**: 1590
10 D'Agostino M *et al*. Phys Lett **B**, 2000, **473**: 219
11 Chomaz Ph *et al*. Phys Rev Lett, 2000, **85**: 3587
12 Schmidt M *et al*. Phys Rev Lett, 2001, **86**: 1191
13 Labastie M, Whetten R L. Phys Rev Lett, 1990, **65**: 1567
14 Borderie B *et al*. Phys Rev Lett, 2001, **86**: 3252
15 Botet R *et al*. Phys Rev Lett, 2001, **86**: 3514
16 Ma Y G. Phys Rev Lett, 1999, **83**: 3617
17 Ma Y G. Chin Phys Lett, 2000, **17**: 340
18 Elliott J B *et al*. Phys Rev Lett, 2002, **88**: 042701; nucl-ex/0205004
19 Elliott J B *et al*. Phys Rev C, 2003, **67**: 24609
20 Richert J, Wagner P. Phys Rep, 2001, **350**: 1
21 Das Gupta S, Mekjian A, Tsang M B. Adv Nucl Phys, 2001, **26**: 91 and references therein
22 Ma Y G, Zhang H Y, Shen W Q. Prog Phys (in Chinese), 2002, **22**: 99
23 Ring P, Schuck P. The nuclear many-body problem, New York: Springer-Verlag, 1980, 5
24 Jaqaman H, Mekjian A Z, Zamick L. Phys Rev, 1983, **C27**: 2782
25 Reif F. Fundamentals of statistical and thermal physics, New York: McGraw Hill, 1965, Chap. 8
26 Gulminelli G *et al*. Phys Rev Lett, 2003, **91**: 202701
27 Raduta Al H, Raduta Ad R. Phys Rev Lett. 2001, **87**: 202701
28 De J N, Das Gupta S, Shlomo S *et al*. Phys Rev **C**, 1997, **55**: R1641
29 Stauffer D, Aharony A. Introduction to percolation theory, Taylor and Francis, London, 1992
30 Bauer W, Dean D R, Mosel U *et al*. Phys Lett **B**, 1985, **150**: 53
31 Bauer W, Post U, Dean D R *et al*. Nucl Phys, 1986, **A 452**: 699
32 Campi X, Desbois J. Invited contribution to the Topical Meeting on "Phase Space Approach to Nuclear Dynamics", Trieste, 1985
33 Campi X. J Phys **A**: Math Gen, 1988, **19**: L917
34 Bondorf J P, Botvina A S, Iljinov A S *et al*. Phys Rep, 1995, **257**: 133
35 Gross D H E. Phys Rep, 1997, **279**: 119
36 Randrup J, Koonin S E. Nucl Phys, 1987, **A471**: 355c
37 Sa B H, Zheng Y M, Zhang X Z. Phys Rev **C**, 1989, **40**: 2680
38 Raduta A H, Raduta A R. Phys Rev, 1997, **C55**: 1344
39 Mekjian A Z. Phys Rev Lett, 1977, **38**: 640
40 Bondorf J P, Donangelo R, Mishustin I M *et al*. Nucl Phys, 1985, **A444**: 460
41 Yang C N, Lee T D. Phys Rev, 1952, **87**: 410
42 Kuo T T S, Ray S, Sharmanna J *et al*. Int J Mod Phys **E**, 1996, **5**: 303
43 Pan J C, Das Gupta S. Phys Rev **C**, 1996, **53**: 1319
44 Das Gupta S *et al*. Nucl Phys, 1997, **A621**: 897
45 Carmona J M, Richert J, Tarancón A. Nucl Phys, 1998, **A643**: 115
46 Chomaz Ph, Gulminelli F. Phys Lett **B**, 1999, **447**: 221
47 Ma Y G *et al*. Eur Phys J A, 1999, **4**: 217
48 Qian W L, Su R K. J Phys **G**, 2003, **29**: 1023
49 Metropolis M *et al*. J Chem Phys, 1953, **21**: 1087
50 Coniglio A, Klein E. J Phys **A**: Math Gen, 1980, **13**: 2775
51 Pan J, Das Gupta S. Phys Rev **C**, 1993, **53**: 1319
52 Stillinger F H, Weber T A. Phys Rev, 1985, **31**: 5262
53 Ma Y G. J Phys **G**, 2001, **27**: 1
54 Verlet L. Phys Rev, 1967, **159**: 98
55 Hirsch A S *et al*. Phys Rev **C**, 1984, **29**: 508
56 Minich R W *et al*. Phys Lett **B**, 1982, **118**: 458
57 Fisher M E. Rep Prog Phys, 1969, **30**: 615
58 Ma Y G, Wada R, Hagel K *et al*. (NIMROD Collaboration: Ma Y G, Wada R, Hagel K, Wang J, Keutgen T, Majka Z, Murray M, Qin L, Smith P, Natowitz J B, Alfaro R, Cibor

J, Cinausero M, El Masri Y, Fabris D, Fioretto E, Kiekies A, Lunardon M, Makeev A, Marie N, Martin E, Martinez-Davalos A, Menchaca-Rocha A, Nebbia G, Prete G, Rizzi V, Ruangma A, Shetty D V, Souliotis G, Staszel P, Veselsky M, Viesti G, Winchester E M, Yennello S J), Arxiv/nucl-ex: 0303016 and long papers, to be published

59 Ma Y G, Wada R, Hagel K *et al*. (NIMROD Collaboration), Ann Report of Cyclotron Institute, Texas A&M University, P. II-18, 2001

60 Gulminelli F, Chomaz Ph. Int J Mod Phys **E**, 1999, **8**: 527

61 Peaslee G F *et al*. Phys Rev **C**, 1994, **49**: R2271

62 Ogilvie C A *et al*. Phys Rev Lett, 1991, **67**: 1214

63 Tsang M B *et al*. Phys Rev Lett, 1993, **71**: 1502

64 Ma Y G, Shen W Q. Phys Rev **C**, 1995, **51**: 710

65 Ma Y G. Eur Phys J **A**, 1999, **6**: 367

66 Zipf GK. Human behavior and the principle of least effort, Addisson-Wesley Press, Cambridge, MA, 1949

67 Turcotte D L. Rep Prog Phys, 1999, **62**: 1377

68 Pan J, Das Gupta S. Phys Rev **C**, 1998, **57**: 1839

69 Dabrowska A *et al*. Acta Phys Polo **B**, 2001, **32**: 3099

70 Ma G L, Ma Y G *et al*. to be published

71 Cole A J. Phys Rev **C**, 2002, **65**: 031601R

72 Sugawa Y, Horiuch H. Prog The Phys, 2001, **105**: 131

73 Chomaz Ph, Gulminelli F, Duflot V. Phys Rev **E**, 2001, **64**: 046114

74 Borderie B. J Phys **G**, 2002, **28**: R217

75 Denbigh K G, Denbigh J S. Entropy in relation to uncomplete knowledge, Cambridge University Press, 1995

76 Brogueira P *et al*. Phys Rev **D**, 1996, **53**: 5283

77 Ma G L, Ma Y G, Wang K *et al*. Chin Phys Lett, 2003, **20**: 1013

78 Stanley H E. Introduction to phase transitions and critical phenomena, Oxford University Press, Cambridge, England, 1992

79 Hauger J A *et al*. Phys Rev **C**, 2000, **62**: 024616

80 Campi X, Krivine H. Z Phys, 1992, **A344**: 81

81 Campi X, Krivine H. Nucl Phys, 1992, **A545**: 161c

82 Dorso C O, Latora V C, Bonasera A. Phys Rev **C**, 1999, **60**: 034606

83 Elattari B, Richert J, Wagner P. Phys Rev Lett, 1992, **69**: 45; Nucl Phys, 1993, **A560**: 603

84 Chomaz Ph, Gulminelli F. Nucl Phys, 1999, **A647**: 153

85 Chomaz Ph, Duflot V, Gulminelli F. Phys Rev Lett, 2000, **85**: 3587

86 D'Agostino M *et al*. Phys Lett **B**, 2000, **473**: 219

87 D'Agostino M *et al*. arXiv:nucl-ex/0310013

88 Botet R, Ploszajczak M. Phys Rev **E**, 2000, **62**: 1825

89 Frankland J D *et al*. ArXiv nucl-ex/0201020

90 Campi X, Krivine H, Plagnol E. Phys Rev **C**, 1994, **50**: R2680

91 Albergo S *et al*. Nuovo Cimento **A**, 1985, **89**: 1

92 Campi X, Krivine H, Plagnol E. Phys Lett **B**, 1996, **385**: 1

93 Ma Y G *et al*. (INDRA Collaboration), Phys Lett **B**, 1997, **390**: 41

94 Borderie B *et al*. Phys Lett **B**, 1996, **388**: 224

95 Borderie B *et al*. Eur Phys J **A**, 1999, **6**: 197

96 Gulminelli F, Durand D. Nucl Phys **A**, 1997, **615**: 117

97 Hagel K *et al*. Nucl Phys, 1988, **A486**: 429

98 Majka Z *et al*. Phys Rev **C**, 1997, **55**: 2991

99 Kwiatkowski K *et al*. Phys Lett **B**, 1998, **423**: 21

100 Cibor J *et al*. Phys Lett **B**, 2000, **473**: 29

101 Natowitz J B, Hagel K, Ma Y G *et al*. Phys Rev **C**, 2002, **66**: 031601(R)

102 Natowitz J B, Hagel K, Ma Y G *et al*. Phys Rev Lett, 2002, **89**: 212701

103 Liu M, Li Z X, Liu J F. Chin Phys Lett, 2003, **20**: 1706

104 Song H Q, Su R K. Phys Rev **C**, 1991, **44**: 2505

105 Zhang L L, Song H Q, Wang P *et al*. Phys Rev **C**, 1999, **59**: 3292

106 Levit S, Bonche P. Nucl Phys, 1985, **A437**: 426

107 Besprovany J, Levitt S. Phys Lett **B**, 1989, **217**: 1

108 Zhang Y J, Su R K, Song H Q *et al*. Phys Rev **C**, 1996, **54**: 1137

109 Das A, Nayak R, Satpathy L. J Phys **G**, 1992, **18**: 869

110 Song H Q, Qian Z X, Su R K. Phys Rev **C**, 1993, **47**: 2001

111 Song H Q, Qian Z X, Su R K. Phys Rev **C**, 1994, **49**: 2924

112 Baldo M, Ferreira L S. Phys Rev **C**, 1999, **59**: 682

113 Bonche P, Levit S, Vautherin D. Nucl Phys, 1985, **A436**: 265

114 Elliott J B *et al*. Phys Rev **C**, 2000, **62**: 064603

115 Youngblood D H, Clark H L, Lui Y W. Phys Rev Lett, 1999, **82**: 691

116 Ogul R, Botivina A S. Phys Rev **C**, 2002, **66**: 051601(R)

117 Karnaukhov V *et al*. Phys Rev **C**, 2003, **67**: 011601(R)

118 Guggenheim E A. J Chem Phys, 1945, **13**: 253

119 D'Agostino M *et al*. Nucl Phys, 1999, **A650**: 329

120 Elliott J B *et al*. Phys Rev **C**, 1997, **55**: 1319

121 Elliott J B *et al*. Phys Rev **C**, 1994, **49**: 3185

122 Pouthas J *et al*. (INDRA Collaboration), Nucl Instr Meth **A**, 1995, **357**: 418

123 Borderie B *et al*. arXiv:nucl-ex/0106007
124 Moretto L G, Wozniak G J. Ann Rev Nucl Part Sci, 1993, **43**: 379 and references therein
125 Colonna M, Chomaz Ph, Ayik S. Phys Rev Lett, 2002, **88**: 12
126 Ayik S, Colonna M, Chomaz Ph. Phys Lett **B**, 1995, **353**: 417
127 Moretto L G *et al*. Phys Rev Lett, 1996, **77**: 2634
128 Tabacaru G *et al*. (INDRA Collaboration), Proc of the XXXVIII Int Winter Meeting on Nuclear Physics, ed Iori I, Moroni A. Ricerca scientifica ed educazione permanente, Bormio, Italy, 2000, 433
129 Borderie B *et al*. (INDRA Collaboration), Phys Rev Lett, 2001, **86**: 3252
130 Le Neindre N *et al*. (INDRA Collaboration), Proc of the XXXVIII Int Winter Meeting on Nuclear Physics, ed Iori I, Moroni A, Ricerca scientifica ed educazione permanente, Bormio, Italy, 2000, 404
131 Chomaz Ph, Gulminelli F. Nucl Phys, 1999, **A647**: 153
132 Li B A, Ko C M, Ren Z. Phys Rev Lett, 1997, **78**: 1644
133 Muller H, Serot B D. Phys Rev **C**, 1995, **52**: 2072
134 Samaddar S K, Das Gupta S. Phys Rev **C**, 2000, **61**: 34610
135 Ma Y G *et al*. Chin Phys Lett, 1999, **16**: 256
136 Ma Y G *et al*. Phys Rev, 1999, **C60**: 24607
137 Dempsey J F *et al*. Phys Rev, 1996, **C54**: 1710
138 Xu H S *et al*. Phys Rev Lett, 2000, **85**: 716
139 Shetty D V *et al*. (NIMROD Collaboration), Phys Rev **C**, 2003, **68**: 054605